European Reviews of Chemical Research

Has been issued since 2014.
ISSN 2312-7708, E-ISSN 2413-7243
2016. Vol.(10). Is. 4. Issued 4 times a year

The journal is registered by Federal Service for Supervision of Mass Media, Communications and Protection of Cultural Heritage (Russian Federation). Registration Certificate **ПИ № ФС77-57042** 25.02.2014.

Journal is indexed by: **CrossRef** (UK), **Electronic scientific library** (Russia), **Journal Index** (USA), **Open Academic Journals Index** (Russia), **ResearchBib** (Japan), **Scientific Indexing Services** (USA)

All manuscripts are peer reviewed by experts in the respective field. Authors of the manuscripts bear responsibility for their content, credibility and reliability.

Editorial board doesn't expect the manuscripts' authors to always agree with its opinion

Postal Address: 26/2 Konstitutcii, Office 6
354000 Sochi, Russian Federation

Website: http://ejournal14.com/en/index.html
E-mail: evr2010@rambler.ru
Founder and Editor: Academic Publishing House *Researcher*

Passed for printing 15.12.16.
Format 21 × 29,7/4.

Headset Georgia.
Ych. Izd. l. 5,1. Ysl. pech. l. 5,8.
Order № 110.

European Reviews of Chemical Research

2016

Is. 4

European Reviews of Chemical Research

European Reviews of Chemical Research

2016 № 4

Издается с 2014 г.
ISSN 2312-7708, E-ISSN 2413-7243
2016. № 4 (10). Выходит 4 раза в год.

Журнал зарегистрирован Федеральной службой по надзору в сфере массовых коммуникаций, связи и охраны культурного наследия (Российская Федерация). Свидетельство о регистрации средства массовой информации **ПИ № ФС77-57042** 25.02.2014.

Журнал индексируется в: **CrossRef** (Великобритания), **Journal Index** (США), **Научная электронная библиотека** (Россия), **Open Academic Journals Index** (Россия), **ResearchBib** (Япония), **Scientific Indexing Services** (США)

Адрес редакции: 354000, Российская Федерация, г. Сочи, ул. Конституции, д. 26/2, оф. 6
Сайт журнала: **http://ejournal14.com**
E-mail: **evr2010@rambler.ru**

Учредитель и издатель: ООО «Научный издательский дом "Исследователь"» - Academic Publishing House *Researcher*

Подписано в печать 15.12.16.
Формат 21 × 29,7/4.

Гарнитура Georgia.
Уч.-изд. л. 5,1. Усл. печ. л. 5,8.
Заказ № 110.

C O N T E N T S

Articles and Statements

Published in the Russian Federation
European Reviews of Chemical Research
Has been issued since 2014.
ISSN: 2312-7708
E-ISSN: 2413-7243
Vol. 10, Is. 4, pp. 102-111, 2016

DOI: 10.13187/ercr.2016.10.102
www.ejournal14.com

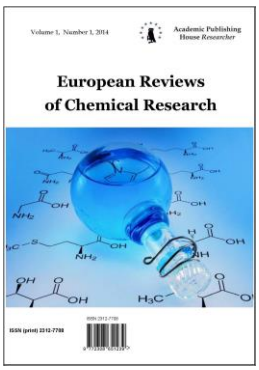

Articles and Statements

UDC 544.7

Catalytic Ignition and Extinction of Hydrogen-Air Mixtures on Platinum Surfaces with Detailed Kinetics and Transport

Junjie Chen [a, *]

[a] Department of Energy and Power Engineering, School of Mechanical and Power Engineering, Henan Polytechnic University, Jiaozuo, Henan, China

Abstract

Surface ignition and extinction of very fuel-lean hydrogen-air mixtures on platinum surfaces were modeled using a detailed surface kinetic mechanism and transport phenomena. A stagnation-point flow geometry was employed to study the effect of heat flux, flow velocity, and composition on the surface ignition and extinction. The temperature and concentration on platinum surfaces as well as the coverage of surface species were also explored to evaluate the role of gas-phase chemistry. It was shown that the platinum surface can be poisoned by different adsorbates, and the dynamic process of surface ignition and extinction is associated with a phase transition from one poisoning species to another. For certain temperatures, multiple poisoned states of the surface coexist. Comparisons of simulations with experiments were carried out, and the results revealed that the self-inhibition of hydrogen surface ignition is caused by poisoning of platinum by atomic hydrogen.

Keywords: surface reaction, surface kinetics, adsorption kinetics, desorption kinetics, platinum surface, catalytic ignition.

1. Introduction

Ignitions, extinctions and multiplicities in surface reactions are important in many applications, including partial oxidation reactors for chemical synthesis and catalytic removal of pollutants. These instabilities delimit the regime of operation of many industrial catalytic reactors and play a major role in reactor safety. Some pathological trends of ignition and extinction have been observed on platinum surfaces. In particular, the self-ignition temperature of carbon monoxide in air rises with feed composition [1], whereas the extinction temperature drops with feed composition. This behavior cannot be explained using a one-step surface reaction with either a positive or a negative order in fuel kinetics. The increase of self-ignition temperature with feed composition, i.e., self-inhibition behavior, has also been observed for hydrogen and olefins but not for paraffins [2]. However, a clear understanding of the reaction mechanism causing this self-

* Corresponding author
E-mail addresses: jgnjie@163.com (J. Chen)

inhibition behavior for some fuels has not been yet achieved.

Previous studies on prototype reaction systems with simple surface chemistry have shown that competition between adsorbates for catalyst sites can result in rate multiplicities and fluctuations [3]. These multiplicities can occur under isothermal conditions where the exothermicity of surface reactions is not a prerequisite as a feedback mechanism. Despite the fact that there are numerous studies on surface multiplicities and phase transitions [4], there are no studies on surface multiplicities of oxidation reactors using detailed surface kinetics. Therefore, how previous results can be generalized for detailed surface reaction mechanisms is still not clear. On the other hand, the advance in surface chemistry for simple adsorbates on some catalysts allows detailed modeling of these systems.

In this work, surface ignition and extinction of very fuel-lean hydrogen-air mixtures on platinum surfaces were studied, using a stagnation point-flow model with detailed surface kinetics. A stagnation-point flow geometry was considered because it is a widely used experimental configuration and makes mathematical analysis tractable. Additionally, it represents a well-defined flow field with a zero-dimensional catalytic surface, which enables coupled modeling of heterogeneous chemistry and reactive flow at steady-state and transient conditions. The flow is towered to a disk by creating a stagnation point on the disk to achieve a thick and uniform deposition across the substrate.

2. Computational methods

A stagnation-point flow geometry is modelled, as shown schematically in Figure 1. Premixed hydrogen-air mixtures impinge on a flat platinum surface. The ideal-gas law is employed as an equation of state. The conservation equations of continuity, momentum, energy, and species for axisymmetric flow are employed. The surface chemistry on the platinum surface is modeled through appropriate mass-transfer boundary conditions. The feed composition is fixed. The composition above the surface, which determines the state of the platinum surface, is an unknown of the problem in the continuum flow regime, given that the mean free path is relatively low, compared to the characteristic dimensions of the reactor. The unknown surface composition is determined from the surface boundary condition of species. Concerning the species boundary conditions, the flux of a gas-phase species at the surface is equal to its net rate of consumption because of interfacial reactions. Interfacial reactions are defined as these reactions which include at least one surface species. For a surface species, at steady state the net reaction rate is equal to zero. Finally, the coverage of vacancies is computed from an overall balance on catalyst sites.

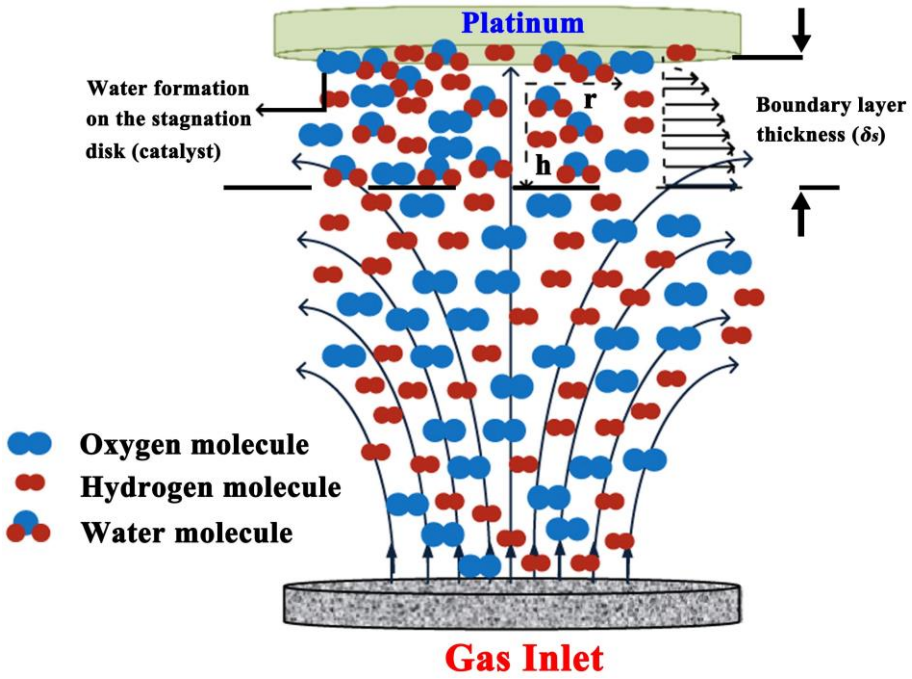

Fig. 1. Schematic diagram of the simulated stagnation flow reactor

Simulations are performed at ambient temperature and atmospheric pressure. A second order finite difference scheme is used to discretize the differential equations. The arc-length continuation techniques and Newton-Raphson method are employed to solve the coupled algebraic equations. A typical simulation involves approximately 10^3 equations and approximately 10^3 unknowns and requires several hours, when parallel processing is used for a one-parameter continuation run.

The surface reaction mechanism of Deutschmann *et al.* [5] is used. The surface mechanism used is of the Langmuir-Hinshelwood type. The stable product in the catalytic oxidation of hydrogen is water. Hydrogen and oxygen dissociate upon adsorption to H* and O*, respectively (* denotes adsorbed species). H* and O* desorb by bimolecular association to form hydrogen and oxygen, respectively. H* reacts with O* to form OH*. Since the desorption of OH* is highly activated, OH* is preferentially converted to H_2O*. H_2O* desorbs readily at relatively low temperatures to form water in the gas phase. Second-order adsorption and desorption kinetics for hydrogen and oxygen are used here. Interfacial reactions include the competitive dissociative adsorption of hydrogen and oxygen, the competitive adsorption of water, the re-combinative desorption of H* and O* into hydrogen and oxygen, respectively, the desorption of H_2O* and OH*, and surface reactions [6]. This mechanism has been tested against experimental ignition data, and good agreement has been found [7]. The gas-phase reaction mechanism of Burke *et al.* [8] is employed, which has been tested against a wide range of combustion targets.

3. Results and discussion

3.1. Surface temperature and concentration

Figure 2 shows the surface temperature and the mole fraction of hydrogen at the gas-surface interface as a function of heat flux. The heat flux is provided to the surface by resistive heating of the platinum foil for 0.8% hydrogen in air [9]. Neither radiation nor heat losses at the back of the platinum foil are considered here because the ignition temperatures are low. At zero power, the surface temperature is equal to ambient temperature. As the power increases, the surface temperature increases almost linearly, and the reactivity of hydrogen is negligible. At a certain critical value of power, a turning point is found, which is indicated with a vertical arrow, where the system ignites. The corresponding temperature is called an ignition temperature.

Upon ignition, the system jumps to the ignited branch. An increase in surface temperature and a decrease in the hydrogen mole fraction will then be observed. In simulations, an intermediate unstable branch connects the ignited and extinguished branches. For reasons of clarity and because of the multiple curves, all branches are drawn using the same marking. As the power increases on the ignited branch, at approximately 1100 K a change in the slope of the surface temperature-heat flux curve can be observed. At this point, the surface mole fraction of hydrogen decreases sharply with the power input to the surface, indicating the onset of gas-phase chemistry.

As the power decreases from high values along the ignited branch, a critical point is reached where surface reactions cannot be further self-sustained. This point corresponds to an extinction indicated by a vertical arrow. The extinction temperature is below ambient temperature for these conditions, i.e. freezing of the surface is needed to extinguish surface reactions. The temperature on the ignited branch where surface reactions can be self-sustained, i.e. at zero power, is called an auto-thermal point. This point divides the space into the freezing and heating subspaces.

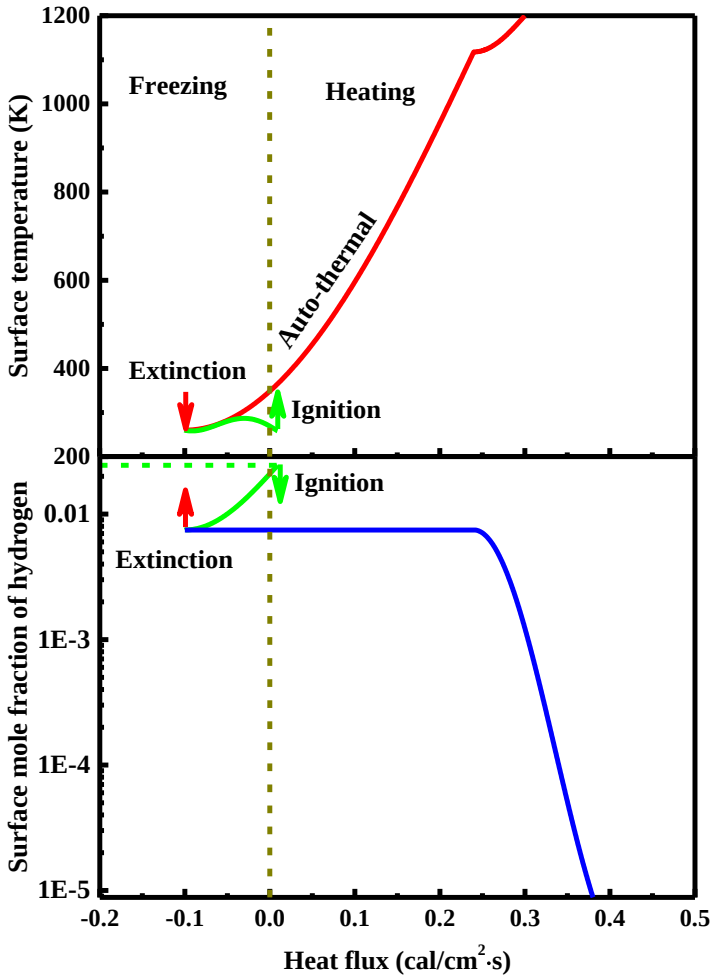

Fig. 2. Effect of heat flux on the surface temperature and the mole fraction of hydrogen at the gas-surface interface. A mixture of 0.8% hydrogen in air with a strain rate of 50 s^{-1} is considered.

3.2. Role of gas-phase chemistry

Until recently, gas-phase chemistry has been generally ignored in simulations, even though experiments have provided evidence towards the presence of vigorous gas-phase reactivity under certain operating conditions [10]. To examine the role of gas-phase chemistry in oxidation, simulations are performed while suppressing gas-phase reactions. Figure 3 shows the effect of gas-phase chemistry on the surface temperature and the mole fraction of hydrogen at the gas-surface interface.

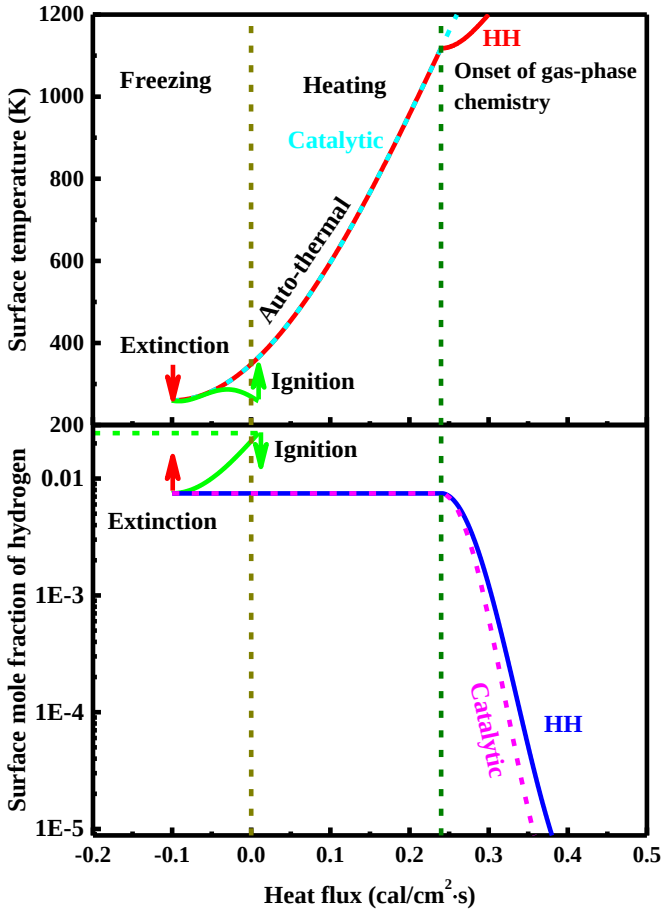

Fig. 3. Effect of gas-phase chemistry on the surface temperature and the mole fraction of hydrogen at the gas-surface interface. The solid lines indicate the coupled homogeneous-heterogeneous (HH) process with gas-phase and surface chemistry, and the dashed lines correspond to the catalytic process alone without gas-phase chemistry.

Gas-phase chemistry has essentially no effect on the catalytic ignition and extinction temperatures. However, deviations between the two simulations, with and without the gas-phase chemistry, can be observed when the surface temperature is above approximately 1100 K. When the mole fraction of hydrogen is plotted versus temperature instead of power, the change in slopes corresponds to an actual turning point, i.e., ignition [11]. This is similar to the homogeneous ignition found in earlier work of Bui *et al.* [12]. Therefore, this change in slope at approximately 1100 K indicates the onset of homogeneous reactions.

3.3. Surface coverage

Figure 4 shows the coverage of surface species as a function of the power input to the surface. For temperatures below the catalytic ignition temperature, the surface is covered with atomic hydrogen H*. Thermodynamically, atomic oxygen is preferred at low temperatures on platinum surfaces compared to atomic hydrogen because of the high heat of adsorption of oxygen [13]. However, the entire system is not in thermodynamic equilibrium [14]. The high rate of adsorption of hydrogen, because of its low molecular mass and its higher sticking coefficient compared to oxygen [15], leads to preferential dissociation of hydrogen. Since the activation energy for desorption of H* is relatively high and the temperatures are low, the fraction of free platinum sites (vacancies) is very low, and oxygen cannot dissociate (an "H*-poisoned" surface). As a result, the surface reaction rates and the conversion of the fuel are low. A similar behavior has been observed in the oxidation of carbon monoxide [16].

Upon ignition, the surface becomes covered with atomic oxygen O*, i.e. during the transient process of catalytic ignition, a phase transition from an H*-covered surface to an O*-covered surface occurs. This transition occurs because during ignition the small fraction of hydrogen becomes almost completely oxidized. Oxygen is then in such an excess above the surface that its

rate of adsorption is higher than that of hydrogen. Therefore, oxygen dissociates to O*. This transition from an H*-covered surface to an O*-covered surface is because of a change in partial pressures of reactants above the surface, as determined by the surface boundary condition. Since the desorption of O* is highly activated, at temperatures below the homogeneous ignition temperature, the surface is partially poisoned by O*. A small fraction of vacancies at intermediate temperatures allows for a small reactivity on this branch.

On the ignited branch, as the power decreases, OH* and H_2O* increase at the expense of O*. Near extinction, i.e., low temperatures, H_2O* cannot desorb and blocks most catalyst sites, i.e., a product poisoning. During extinction, the surface converts from (H_2O* + OH*)-blocked to H*-blocked.

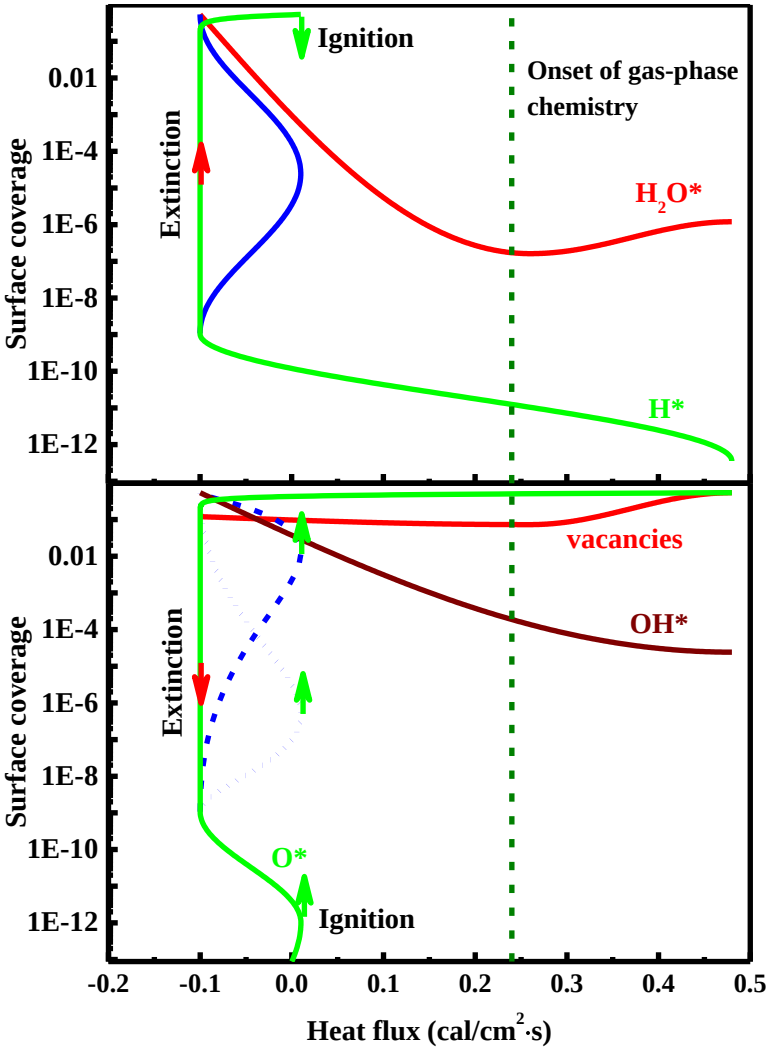

Fig. 4. Effect of heat flux on the surface coverage of species for the coupled homogeneous-heterogeneous process. Upon ignition, a transition from an H*-covered surface to an O*-covered surface occurs. Upon extinction, a transition from an H_2O*-covered surface to an H*-covered surface occurs.

The simulations reveal that the multiple poisoned phases can coexist at the same temperature. Outside the multiplicity regime, the surface is covered by one of the adsorbents (H* or O*), and within the multiplicity regime, the surface can be covered by one of the adsorbents, the product (H_2O*), and an intermediate (OH*).

3.4. Effect of flow velocity

The above simulations are performed for 0.8% hydrogen in air. In this section, the effect of flow velocity on the catalytic ignition temperature is examined, and the results are compared with experiments. At similar compositions, the catalytic ignition temperature is higher than

experimental data. Sensitivity analysis reveals that the catalytic ignition temperature is affected mainly by the activation energy for desorption of H*, and the sticking coefficients of hydrogen and oxygen (data not shown). As an example of illustrating the role of desorption of H*, simulations are performed for different activation energies. Figure 5 shows the effect of flow velocity on the catalytic ignition temperature. The results are obtained from simulations using detailed chemistry by varying the strain rate, i.e., a velocity gradient outside the boundary layer [17]. For a nozzle at a fixed distance from the platinum surface, the flow velocity in simulations is proportional to the strain rate. The experimental results are obtained on platinum wires by restricting the flow to the low Reynolds number range [18].

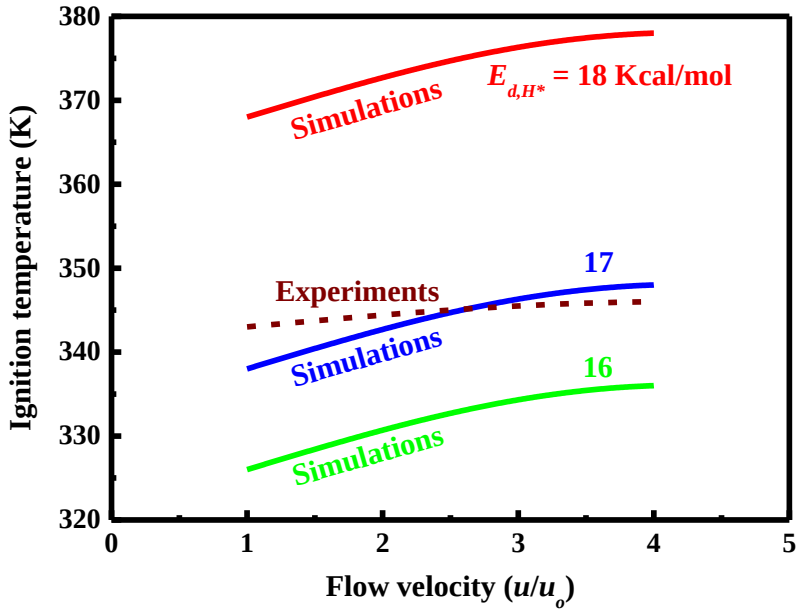

Fig. 5. Effect of flow velocity on the catalytic ignition temperature. A mixture of 0.8% hydrogen in air for three values of activation energy of desorption of H* is considered. The experimental results are obtained on platinum wires by restricting the flow to the low Reynolds number range. The scaling strain rate in the simulations is 50 s^{-1}, and the scaling velocity in the experiments is 5 $cm \cdot s^{-1}$.

Simulations show a slight increase in ignition temperature with the increase of flow velocity. However, both simulations and experiments indicate that the effect of transport phenomena on the catalytic ignition temperature is minor for these conditions, i.e. kinetics controls catalytic ignition. A different activation energy for desorption shifts the ignition curve but does not change the qualitative response of the system.

3.5. Effect of composition

In this section, the effect of composition on the catalytic ignition temperature is examined, and the results are compared with experiments. Figure 6 shows the effect of composition on the catalytic ignition temperature. Experimentally, the self-inhibition of hydrogen on its ignition temperature can be observed [19]. The experimentally observed trend of increasing ignition temperature with increasing hydrogen to oxygen ratio can be attributed to a combination of the hydrogen desorption kinetics and a weaker coverage dependence for hydrogen sticking than for oxygen sticking on the surface [20]. For example, The catalytic ignition temperature is determined by a competition between hydrogen site blocking on the surface and hydrogen desorption, which makes the catalytic ignition temperature increase with increasing hydrogen to oxygen ratio [21]. Additionally, the catalytic ignition of hydrogen is primarily governed by coupling between the heat balance, the kinetics of adsorption of hydrogen and oxygen, and the desorption kinetics of hydrogen [22]. Detailed chemistry predicts correctly this trend independently of the details of the reaction rate constants as far as the surface is blocked by H* before ignition occurs.

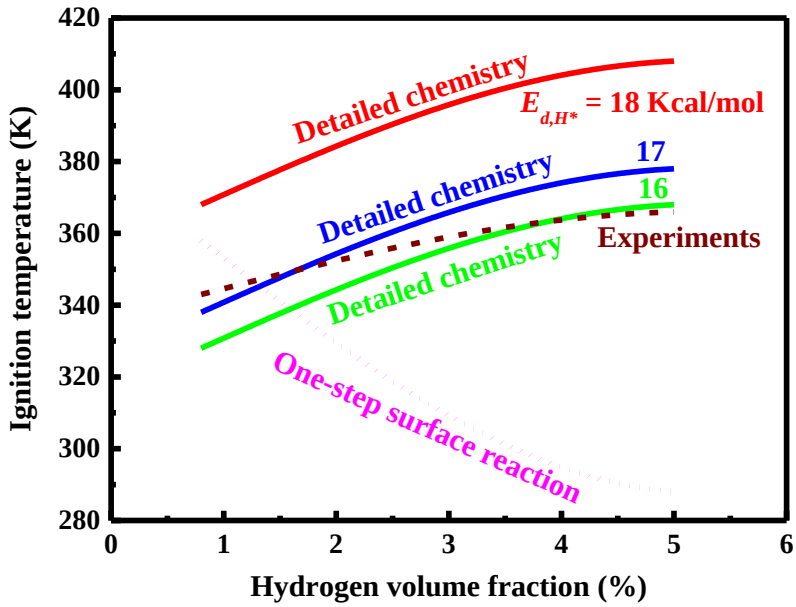

Fig. 6. Effect of composition on the catalytic ignition temperature of hydrogen. The experimental results are obtained on platinum wires by restricting the flow to the low Reynolds number range.

Simulations have also been performed using a one-step surface chemistry. The rate of the global surface reaction is taken to be first order with respect to hydrogen and zero order with respect to oxygen, as suggested experimentally [23]. The pre-exponential and activation energy are adjusted so that ignition happens at a positive power [24], and the catalytic ignition temperature is close to experiments for 0.8% hydrogen in air [25]. The rate expression can be found in the previous work of Ikeda *et al.* [26], in which the interaction between heterogeneous and homogeneous reactions arising when a mixture of hydrogen and air impinges on a platinum plate at elevated temperature has been studied. The relevant kinetics parameters can be found in the previous work of Petersson and Ackelid [27] as well as Johansson *et al.* [28].

The one-step surface chemistry predicts the opposite trend from the experimental results. This promotion of ignition with composition is because of the fact that in the case of a global reaction, the catalytic ignition is caused by the exothermicity of the surface reaction. As the composition increases, more heat is released from the surface reactions, and thus the catalytic ignition occurs at lower temperatures. Qualitatively, the promotion of catalytic ignition with composition is insensitive to the details of the parameters of the one-step surface kinetics.

It has been found that the catalytic ignition of hydrogen is controlled by the slow desorption of H* and the availability of free platinum sites. Therefore, the self-inhibition of hydrogen on its ignition is caused by an increase in the partial pressure of hydrogen above the surface with increasing composition, which results in a more effective blocking of platinum. A higher surface temperature is then needed for desorption of H* to occur. Given the fact that the surface chemistry has been derived mainly at low pressures and is used here at atmospheric pressure, the qualitative agreement between experiments and simulations is very good. Here, the kinetics parameters do not adjust to fit the experimental data; rather, it is illustrated that self-inhibition is caused by blocking of the catalyst by the fuel or one of its fragments for more complex hydrocarbons. Improvements between simulations and experiments by including adsorbate-adsorbate interactions may also be possible.

4. Conclusion

The catalytic ignition and extinction of very fuel-lean hydrogen-air mixtures on platinum surfaces were studied, using a stagnation point-flow model with detailed surface kinetics. The main points can be summarized as follows. There is a small effect of transport on the catalytic ignition for the regime of flow velocities studied. The self-inhibition behavior found experimentally is also reproduced in simulations, and has been attributed to partial poisoning of the catalyst by atomic hydrogen at low temperatures. Catalytic ignition is controlled by desorption of atomic hydrogen.

Upon ignition, the surface becomes poisoned by atomic oxygen until at higher temperatures homogeneous ignition takes place, i.e., the onset of the gas-phase ignition. Near extinction, the surface is poisoned by the product water. These surface phase-transitions occur as the temperature and/or the partial pressures of reactants, i.e., composition, change because of a competition of adsorbates for catalyst sites. Coexistence of various poisoned states by intermediates and the product have been observed, using a mean-field model. The future work will focus on the role of surface reaction mechanisms, transport, and reaction exothermicity in catalytic ignition.

5. Acknowledgement

This work was supported by the National Natural Science Foundation of China (No. 51506048).

References

1. Cardoso M.A.A. and Luss D. Stability of catalytic wires. *Chemical Engineering Science*, Volume 24, Issue 11, 1969, pp. 1699-1710.

2. Trinchero A., Hellman A., and Grönbeck H. Methane oxidation over Pd and Pt studied by DFT and kinetic modeling. *Surface Science*, Volume 616, 2013, pp. 206-213.

3. Zhdanov V.P. Impact of surface science on the understanding of kinetics of heterogeneous catalytic reactions. *Surface Science*, Volume 500, Issues 1-3, 2002, pp. 966-985.

4. Enterkin J.A., Becerra-Toledo A.E., Poeppelmeier K.R., and Marks L.D. A chemical approach to understanding oxide surfaces. *Surface Science*, Volume 606, Issues 3-4, 2012, pp. 344-355.

5. Deutschmann O., Maier L.I., Riedel U., Stroemman A.H., and Dibble R.W. Hydrogen assisted catalytic combustion of methane on platinum. *Catalysis Today*, Volume 59, Issues 1-2, 2000, pp. 141-150.

6. Karakaya C., Deutschmann O. Kinetics of hydrogen oxidation on Rh/Al_2O_3 catalysts studied in a stagnation-flow reactor. *Chemical Engineering Science*, Volume 89, 2013, pp. 171-184.

7. Sui R., Prasianakis N.I., Mantzaras J., Mallya N., Theile J., Lagrange D., and Friess M. An experimental and numerical investigation of the combustion and heat transfer characteristics of hydrogen-fueled catalytic microreactors. *Chemical Engineering Science*, Volume 141, 2016, pp. 214-230.

8. Burke M.P., Chaos M., Ju Y., Dryer F.L., and Klippenstein S.J. Comprehensive H_2/O_2 kinetic model for high-pressure combustion. *International Journal of Chemical Kinetics*, Volume 44, Isue 7, 2012, pp. 444-474.

9. Bui P.-A., Vlachos D.G., and Westmoreland P.R. Modeling ignition of catalytic reactors with detailed surface kinetics and transport: Oxidation of H_2/air mixtures over platinum surfaces. *Industrial & Engineering Chemistry Research*, Volume 36, Issue 7, 1997, pp. 2558-2567.

10. Schultze M., Mantzaras J., Bombach R., and Boulouchos K. An experimental and numerical investigation of the hetero-/homogeneous combustion of fuel-rich hydrogen/air mixtures over platinum. *Proceedings of the Combustion Institute*, Volume 34, Issue 2, 2013, pp. 2269-2277.

11. Vlachos D.G. and Bui P.-A. Catalytic ignition and extinction of hydrogen: comparison of simulations and experiments. *Surface Science*, Volume 364, Issue 3, 1996, pp. L625-L630.

12. Bui P.-A., Vlachos D.G., and Westmoreland P.R. Catalytic ignition of methane/oxygen mixtures over platinum surfaces: comparison of detailed simulations and experiments. *Surface Science*, Volume 385, Issues 2-3, 1997, pp. L1029-L1034.

13. Ikeda H., Sato J., and Williams F.A. Surface kinetics for catalytic combustion of hydrogen-air mixtures on platinum at atmospheric pressure in stagnation flows. *Surface Science*, Volume 326, Issues 1-2, 1995, pp. 11-26.

14. Ljungström S., Kasemo B., Rosen A., Wahnström T., and Fridell E. An experimental study of the kinetics of OH and H_2O formation on Pt in the $H_2 + O_2$ reaction. *Surface Science*, Volume 216, Issues 1-2, 1989, pp. 63-92.

15. Anton A.B. and Cadogan D.C. The mechanism and kinetics of water formation on Pt(111). *Surface Science*, Volume 239, Issue 3, 1990, pp. L548-L560.

16. Aal S.A. CO catalytic oxidation on Pt-doped single wall boron nitride nanotube: first-principles investigations. *Surface Science*, Volume 644, 2016, pp. 1-12.

17. Vlachos D.G., Schmidt L.D., and Aris R.. Ignition and extinction of flames near

surfaces: Combustion of H_2 in air. *Combustion and Flame*, Volume 95, Issue 3, 1993, pp. 313-335.

18. Cho P. and Law C.K. Catalytic ignition of fuel/oxygen/nitrogen mixtures over platinum. *Combustion and Flame*, Volume 66, Issue 2, 1986, pp. 159-170.

19. Norton D.G. and Vlachos D.G. Hydrogen assisted self-ignition of propane/air mixtures in catalytic microburners. *Proceedings of the Combustion Institute*, Volume 30, Issue 2, 2005, pp. 2473-2480.

20. Fassihi M., Zhdanov V.P., Rinnemo M., Keck K.E., and Kasemo B. A theoretical and experimental study of catalytic ignition in the hydrogen-oxygen reaction on platinum. *Journal of Catalysis*, Volume 141, Issue 2, 1993, pp. 438-452.

21. Rinnemo M., Fassihi M., and Kasemo B. The critical condition for catalytic ignition. H_2/O_2 on Pt. *Chemical Physics Letters*, Volume 211, Issue 1, 1993, pp. 60-64.

22. Rinnemo M., Deutschmann O., Behrendt F., and Kasemo B. Experimental and numerical investigation of the catalytic ignition of mixtures of hydrogen and oxygen on platinum. *Combustion and Flame*, Volume 111, Issue 4, 1997, pp. 312-326.

23. Appel C., Mantzaras J., Schaeren R., Bombach R., Kaeppeli B., and Inauen A.. An experimental and numerical investigation of turbulent catalytically stabilized channel flow combustion of hydrogen/air mixtures over platinum. *Proceedings of the Combustion Institute*, Volume 29, Issue 1, 2002, pp. 1031-1038.

24. Appel C., Mantzaras J., Schaeren R., Bombach R., Inauen A., Kaeppeli B., Hemmerling B., and Stampanoni A.. An experimental and numerical investigation of homogeneous ignition in catalytically stabilized combustion of hydrogen/air mixtures over platinum. *Combustion and Flame*, Volume 128, Issue 4, 2002, pp. 340-368.

25. Appel C., Mantzaras J., Schaeren R., Bombach R., and Inauen A. Turbulent catalytically stabilized combustion of hydrogen/air mixtures in entry channel flows. *Combustion and Flame*, Volume 140, Issues 1-2, 2005, pp. 70-92.

26. Ikeda H., Libby P.A., and Williams F.A. Catalytic combustion of hydrogen-air mixtures in stagnation flows. *Combustion and Flame*, Volume 93, Issues 1-2, 1993, pp. 138-148.

27. Petersson L.-G. and Ackelid U. Kinetic studies of diffusion limited gas-surface reactions by spatially resolved gas sampling: reaction rates and sticking coefficients in the $H_2 + O_2$ reaction on Pt. *Surface Science*, Volumes 269-270, 1992, pp. 500-505.

28. Johansson Å., Försth M., and Rosén A. A comparative study of high-temperature water formation and OH desorption on polycrystalline palladium and platinum catalysts. *Surface Science*, Volume 529, Issues 1-2, 2003, pp. 247-266.

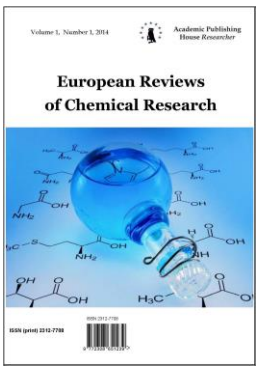

Published in the Russian Federation
European Reviews of Chemical Research
Has been issued since 2014.
ISSN: 2312-7708
E-ISSN: 2413-7243
Vol. 10, Is. 4, pp. 112-121, 2016

DOI: 10.13187/ercr.2016.10.112
www.ejournal14.com

UDC 544.4.032.7

Kinetic Features of Cadmium Sulfide Deposition from Aqueous Solutions with Various Ligand Backgrounds

Natalia A. Forostyanaya [a, *], Anastasia D. Kutyavina [a], Larisa N. Maskaeva [a], Vyacheslav F. Markov [a]

[a] Ural Federal University named after the first President of Russia B.N. Yeltsin, Ekaterinburg, Russian Federation

Abstract

A comparative kinetic study was carried out and formal kinetic equations were derived for the chemical deposition of cadmium sulfide from aqueous solutions containing various cadmium complexes onto a glass-ceramic substrate by thiourea under conditions of spontaneous nucleation and interfacial area control. The morphology of the resultant films were examined, on this basis their nanostructure nature was confirmed, taking into account the data on crystallite size analysis.

Keywords: hydrochemical synthesis, cadmium sulfide, chemical kinetics, spontaneous nucleation of solid phase, thin films, surface morphology.

1. Introduction

Cadmium sulfide is the most known direct-bandgap A_2B_6 semiconductor with the forbidden band gap of 2.42 eV, which has for long attracted interest [1]. It has found microelectronic and optoelectronic applications, in particular in light-emitting diodes, lasers, photoelectric converters, solar cells etc. [2–6].

Among the variety of methods used to produce layers for cadmium sulfide-based photovoltaic cells such as vacuum evaporation and condensation in a quasiclosed volume [7], vacuum condensation from a vapor phase [8], pulverization followed by pyrolysis [9] the method of chemical bath deposition of films by thiourea from aqueous solutions of cadmium salts is the most promising [10]. Its attractive features include mild conditions of the preparation of cadmium sulfide layers, low deposition temperature (≤353 K), high controllability of the film thickness, and easy modifiability of the film composition and morphology.

Despite the above-mentioned advantages, some technological details of the chemical bath deposition method occasionally hinder the preparation of high-quality cadmium sulfide films, but the functional properties and microstructural characteristics of cadmium sulfide layers should be provided as early as in the hydrochemical synthesis stage.

At the first time hydrochemical deposition of CdS films by thiourea has been studied in the Mokrushin and Tkachev works [11], and the conditions of their formation have been described in

* Corresponding author
E-mail addresses: n.a.forostianaia@urfu.ru (N.A. Forostyanaya), n-kutyavina@mail.ru (A.D. Kutyavina), mln@ural.ru (L.N. Maskaeva), v.f.markov@ustu.ru (V.F. Markov)

[12, 13]. The complexing agent for cadmium in those studies was ammonia. More recent studies employed Trilon B [14], ethylenediamine [15], trisodium citrate [16], and amino acids [17] as ligands. Previously, we have performed thermodynamic evaluation of the conditions of formation of solid CdS phase by chemical bath deposition [18]. One of the most important factors influencing the CdS composition and structure is the ligand background created in the reaction system. The stability of the resulting complex metal species and of the spatial structure of the ligand affect both the size of the emerging nuclei and their interactions, which ultimately produce a decisive effect on the micro-structure and morphology of the films synthesized. However, those studies did not report on the rate of formation of the solid phase under conditions of spontaneous nucleation and on the ways of its control with the aim to actively influence the morphology, structure, and electrophysical properties of the deposited films.

As shown in [10], hydrochemical deposition of metal sulfides is a heterogeneous autocatalytic process in which the function of catalyst it fulfilled by the metal sulfide phase formed on the reactor wall surface, on the substrate, or in the reaction mixture volume. Importantly, under conditions of spontaneous nucleation and significant supersaturation the reaction between the sulfidizer and soluble cadmium salt leads to the CdS solid phase formation not only on the substrate surface but also, to a considerable extent, in the reaction mixture volume (as a powdery precipitate).

Here we report about the kinetic features of cadmium sulfide chemical bath deposition by thiourea from solutions with different ligand background under conditions of spontaneous nucleation and control of the solid phase surface area. Kinetic studies aim mainly to identify the role played and contribution made by each component of the reaction mixture to the process rate and to determine how it is affected by the temperature and interfacial area. To this end it is necessary to estimate the partial orders of the CdS formation reaction with respect to all the reactants and the apparent activation energy.

2. Experimental

The reaction mixtures for the hydrochemical deposition were prepared from 2.0 M thiourea (CSN_2H_4, ultrapure grade), 1.0 M cadmium chloride ($CdCl_2$, chemically pure grade), 1.5 M trisodiumcitrate ($Na_3C_6H_5O_7$, ultrapure grade), 13 M aqueous ammonia (NH_4OH, chemically pure grade), and 5 M potassium hydroxide KOH, pH of the solutions was monitored with a pH-121 pH-meter.

For the preparation of the reaction mixtures the reactants were mixed in a strictly specified sequence: to a cadmium salt solution the complexing agent was added and next the calculated amount of water, and this was followed by introduction of the alkaline agent (in citrate system) and then of thiourea. The temperature of the stock solutions during the preparation of the reaction mixtures was 293 K. The CdS deposition was carried out in molybdenum glass reactors which were placed in a TS–TB–10 thermostat.

The kinetic research of the cadmium sulfide deposition under spontaneous nucleation conditions over 308–333 K temperature range for three different formulations of the reaction mixture with the total content of cadmium chloride ($CdCl_2$) and thiourea (CSN_2H_4) of 0.005–0.02 and 0.20–0.60 M, respectively. The first reaction mixture contained citrate ions $C_6H_5O_7^{3-}$ (citrate system), using trisodium citrate Na_3Cit (0.10–0.40 M) as the main complexing agent, the second mixture, aqueous ammonium hydroxide NH_4OH (ammonia system) with concentration 1.0–3.0 M, and the third mixture, both ligands at varied citrate and ammonia concentrations (ammonia-citrate system). For creation of an alkaline medium, KOH was introduced into the citrate reaction bath to pH 11.8; in the two other systems, aqueous ammonium hydroxide whose concentration provided pH from 11.2 to 12.2 served as alkaline agent. The kinetic features of the cadmium sulfide deposition under control of the surface area of the solid phase being formed were studied in the ammonia-citrate system.

The kinetic features of the hydrochemical deposition of the solid phase of cadmium sulfide were studied by the excess concentration method [23]. The changes in the cadmium salt concentration in the reaction mixture were monitored by periodic sampling and analysis of the samples taken by trilonometric back titration using Eriochrome Black T indicator and a buffer solution (pH = 10) [24].

For studying the process kinetics under a controlled interfacial area we used glass powder with an average particle size of 80 μm, previously coated with a chemically deposited cadmium

sulfide layer. The shape of the powder particles was taken as spherical. The surface area contacting the solution was calculated as the sum of the surface area of the reactor walls S_r = 0.0221 m^2 and the surface area per unit mass of the glass powder $S_{gl.p.}$ = 0.0305 m^2/g which was calculated using the glass powder density (2.45 g/cm^3). The powder particles were kept in suspension by conducting the experiments in a vertically rotating reactor at 10 rpm.

The CdS films were deposited onto 30×24 mm sitall substrates ST-50-1 previously degreased in sulfochromic solution [24]. The thickness of the films deposited was measured by an MII-4M Linnik interferometer.

The initial and final stages of the crystallization of the semiconductor CdS layer were examined by scaning electron microscopy (SEM) using the Scanning Electron Mucroscope JEOL JSM-5900LV and atomic force microscopy (AFM) using a Ntegra Prima (Russia, NT-MDT) and an Asylum MFP-3D (Asylum, United States) scanning probe microscopes. Scanning was performed in the tapping mode in air at room temperature. The resulting surface images (1×1 μm scan area) served for studying the structure of individual globules and for determining the statistical values of the surface parameters, which were quantitatively estimated by computer image processing in Gwyddion program.

3. Results and discussions

The choice of specific concentration and temperature limits in this work was dictated by the results of the preliminary experiments and of the calculations of the CdS formation conditions [18].

Typical kinetic curves of the cadmium sulfide deposition under conditions of spontaneous nucleation of the solid phase from the three reaction systems studied at the initial concentration of the metal salt of 0.01 M and the thiourea concentration of 0.4 M are shown in Figure 1. It is seen that the deposition is characterized by a negligible induction period, with rate that determined by the concentration of the ligands introduced into the reaction mixture. Increase in the ligand concentration in all the systems slows down the conversion of the cadmium salt to CdS. The cadmium sulfide deposition proceeds less intensively in the citrate system: the reaction attains equilibrium within the first 60 min at [Na_3Cit] = 0.1 M (Fig. 1a, curve 1). The residual concentration of the cadmium ions ($0.55 \cdot 10^{-2}$ M) increases to $0.7 \cdot 10^{-2}$ M under 4-fold increase in the citrate concentration in solution (Fig. 1a, curve 3). This is due to a relatively high stability of the $Cd(OH)Cit^{2-}$ complex of cadmium (pk_i = 9.3 [19]). In the ammonia and ammonia-citrate reaction baths (Figs. 1b–1d) the CdS deposition proceeds to lower residual metal concentrations. This can be explained by a lower degree of cadmium complexation by ammonia (pk_i of the ammonia metal complexes is lower than that of the hydroxycitrate complex) and, on the other hand, by increase in the NH_4OH concentration in solution and in pH, leading to acceleration of the hydrolytic decomposition of thiourea.

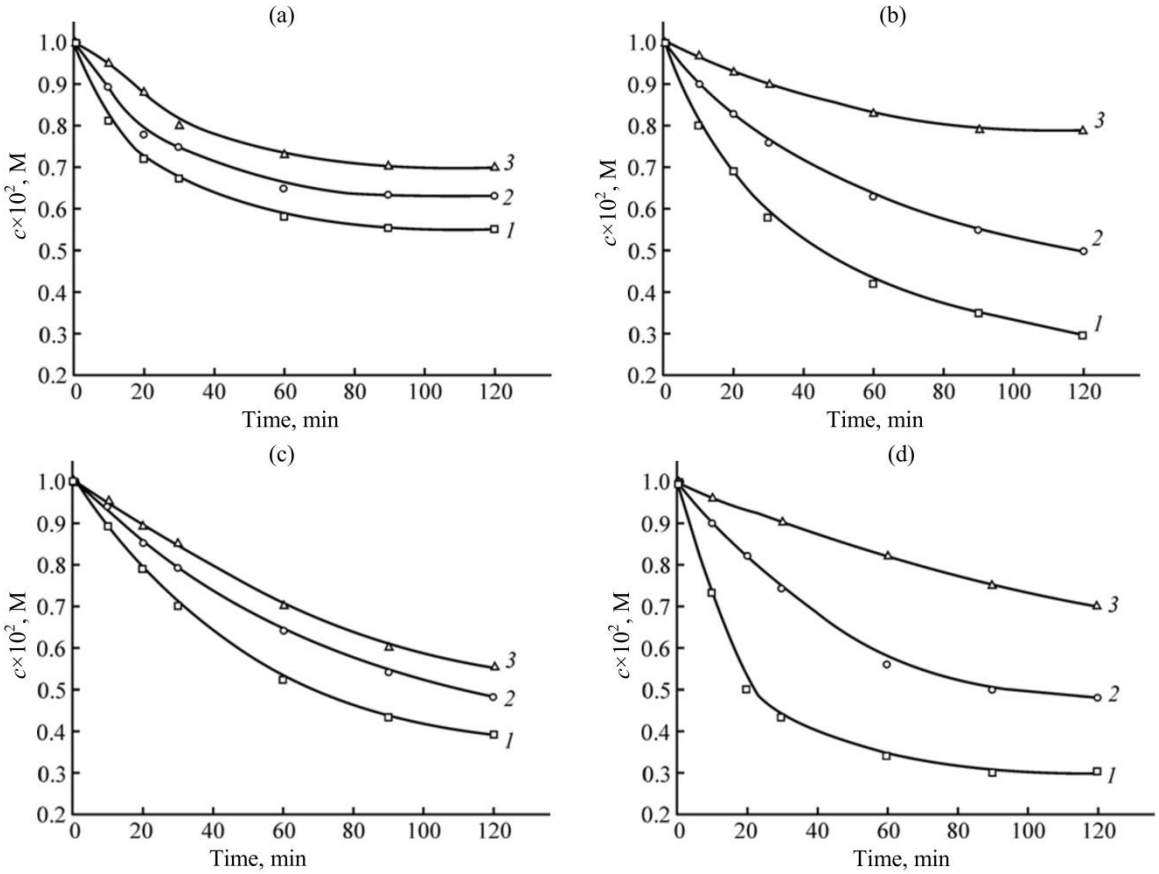

Fig. 1. Kinetic curves of the CdS deposition at 323 K from reaction mixtures of various compositions: (a) citrate, [Na_3Cit], M: (1) 0.1, (2) 0.2, and (3) 0.4, (b) ammonia, [NH_4OH], M: (1) 2.0, (2) 3.0, and (3) 4.0, and (c, d) ammonia-citrate: (c) [Na_3Cit], M: (1) 0.1, (2) 0.2, and (3) 0.4 and [NH_4OH] = 2.0 M and (d) [NH_4OH], M: (1) 1.0, (2) 2.0, and (3) 3.0 and [Na_3Cit] = 0.1 M. Initial $CdCl_2$ and CSN_2H_4 concentrations, 0.01 and 0.4 M, respectively.

The processing of the experimental data of kinetic in the $\ln C_{Cd} - \tau$ coordinates revealed the first order with respect to the metal salt concentration for all the reaction systems tested.

Figure 2, for example, presents typical kinetic curves describing the conversion of the cadmium salt to sulfide in the ammonia system in the 303–323 K range. It is seen that the conversion rate is strongly temperature dependent. After 120 min of synthesis at 303 K the residual cadmium concentration in the presence of 0.4 M thiourea and 3.0 M ammonia was ~80% of the initial level, and at 323 K it was 2.7 times lower.

By constructing the Arrhenius plots we determined the activation energies (E_a) of the CdS deposition in different reaction systems and the pre-exponential factors of the equation. Calculated apparent activation energies of cadmium sulfide deposition in the citrate, ammonia, and ammonia-citrate systems and pre-exponential factors are respectively 39.16, 55.25, 63.34 kJ/mol and $1.7 \cdot 10^3$, $2.6 \cdot 10^3$, $1.1 \cdot 10^7$. The E_a data obtained indicate that the process of deposition proceeds in the kinetic regime. It can be assumed that, because of a relatively low energy barrier to nucleation, the deposition in the citrate system will be accompanied by the formation of a large number of primary CdS particles, as predicted earlier by our thermodynamic calculations [18].

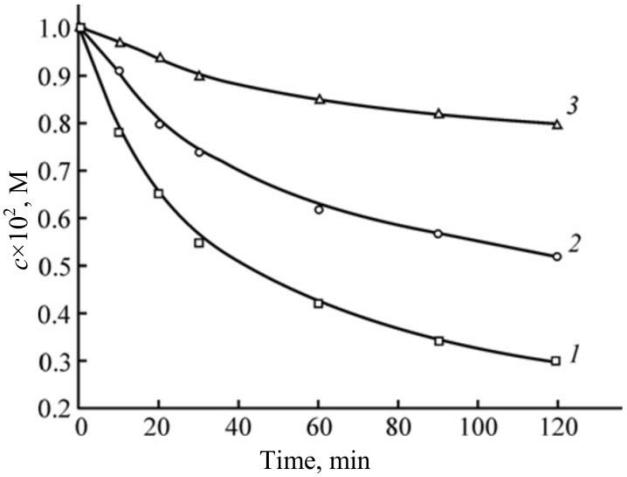

Fig. 2. Kinetic curves of the cadmium salt conversion to CdS at (1) 323, (2) 313, and (3) 303 K. Concentrations of the reactants in the reaction mixture, M: $[CdCl_2]$ = 0.01, $[NH_4OH]$ = 3.0, $[CS(NH_2)_2]$ = 0.4.

Using the partial kinetic orders of all reactants, obtained from our kinetic studies, we derived the formal kinetic equations for the conversion of the cadmium salt to CdS solid phase (W_{CdS}) under spontaneous nucleation in all the systems tested. Although not revealing the actual mechanism of the reaction of the cadmium salt with thiourea, eqs. (1) – (3) generally describe the rate of conversion.

$$W_{CdS(C_6H_5O_7^{3-})} = 1.7 \cdot 10^3 \cdot exp\left(-\frac{39160}{8.314 \cdot T}\right) \cdot C_{Na_3Cit}^{-0.4} \cdot C_{CS(NH_2)_2}^{0.7} \cdot (x_\infty - x) \quad (1)$$

$$W_{CdS(NH_3)} = 2.6 \cdot 10^3 \cdot exp\left(-\frac{55250}{8.314 \cdot T}\right) \cdot C_{NH_3}^{-1.7} \cdot C_{CS(NH_2)_2}^{0.3} \cdot (x_\infty - x) \quad (2)$$

$$W_{CdS(C_6H_5O_7^{3-}+NH_3)} = 1.1 \cdot 10^7 \cdot exp\left(-\frac{63340}{8.314 \cdot T}\right) \cdot C_{Na_3Cit}^{-0.5} \cdot C_{NH_3}^{-1.1} \cdot C_{CS(NH_2)_2}^{2.0} \cdot (x_\infty - x) \quad (3)$$

Here, x_∞, x are the cadmium concentrations at the equilibrium established in the reaction mixture (τ_∞) and at any arbitrary time (τ), respectively, and C_{Na_3Cit}, C_{NH_3}, $C_{CS(NH_2)_2}$ are initial concentrations of trisodium citrate, ammonia, and thiourea, respectively.

Equations (1) – (3) and the data calculated show that temperature and thiourea concentration are the most flexible process parameters for controlling the rate of CdS solid phase formation over fairly broad ranges. The effect from an increase in the thiourea concentration in the reaction bath on the cadmium sulfide deposition rate is especially noticeable in the case of the ammonia-citrate system for which the partial order of the reaction with respect to $CS(NH_2)_2$ was estimated at 2.0 against 0.7 for the citrate and 0.3 for the ammonia systems. In all cases the ligands produce an inhibitory effect on the CdS formation as indicated by the negative partial kinetic orders.

A nontrivial, in our opinion, route consists in the CdS solid phase deposition onto a known surface area (under surface area control). Here, this was achieved by introducing into the reactor of a strictly measured weighed portion of the glass powder classified into a size group with an average particle size of 80 μm, previously coated with cadmium sulfide. With this technique the probability of spontaneous nucleation of the solid phase in the solution volume is negligible and the process is localized on the powder particles introduced into the solution. The surface area increases insignificantly due to the sulfide film growth on the powder particles, and the catalytic surface area in the course of the experiment is virtually constant.

Figure 3 shows the kinetic curves describing how the cadmium salt concentration in the ammonia-citrate reaction mixture changes upon introduction of 3, 6, and 10 g of the classified glass powder coated with a CdS film. For comparison, 6 g of the glass powder without predeposited cadmium sulfide layer was introduced into solution. At the surface area of the reactor walls of 0.0221 m² and the per unit mass surface area of the glass powder of 0.0305 m²/g the interfacial area was estimated at 0.1136, 0.2051, and 0.3271 m², respectively. In the last case the spontaneous nucleation of the solid phase in the solution volume was negligible and the process was localized on the surface of the powder particles coated with CdS.

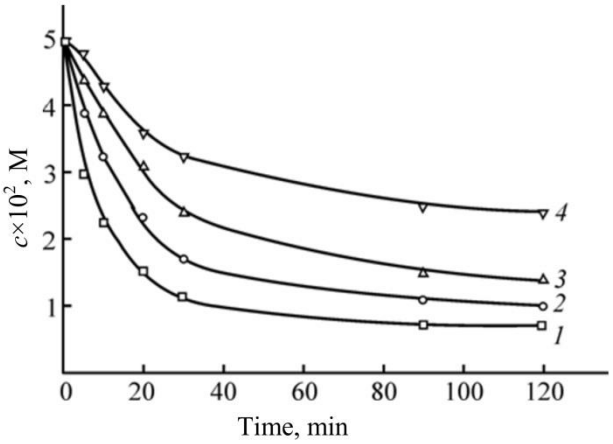

Fig. 3. Kinetic curves of the cadmium salt conversion to CdS upon introduction into the reaction mixture of (4) 6 g of classified glass powder and (3–1): (3) 3, (2) 6, and (1) 10 g of the glass powder previously coated with CdS. Concentrations of the reactants in the reaction mixture, M: $[CdCl_2]$ = 0.005, $[NH_4OH]$ = 3.0, $[Na_3Cit]$ = 0.1, $[CS(NH_2)_2]$ = 0.4; T = 318 K.

As seen from Fig. 3, in the presence of the glass powder previously coated with a cadmium sulfide film the deposition proceeds more intensively (curve 2) than in the presence of an identical amount of pure glass powder (curve 4). An increase in the weighed portion of the powder sample introduced in the glass reactor from 3 to 10 g causes a proportional increase in the CdS deposition rate (curves 1–3). These findings confirm the autocatalytic nature of the chemical bath deposition of cadmium sulfide by thiourea and demonstrate an expressed dependence of the CdS deposition rate on the interfacial area.

Using the results of the complex kinetic studies on CdS deposition in the ammonia-citrate system with interfacial area (S) controlled by introduction of the glass powder coated with a cadmium sulfide film into the reactor we derived formal kinetic equation linking the cadmium sulfide formation rate W_{CdS} with the deposition conditions:

$$W_{CdS(C_6H_5O_7^{3-}+NH_3)} = 6.6\cdot10^3\cdot exp\left(-\frac{47870}{8.314\cdot T}\right)\cdot S\cdot C_{Na_3Cit}^{-0.8}\cdot C_{NH_3}^{-1.3}\cdot C_{CS(NH_2)_2}^{0.2}(x_\infty - x) \quad (4)$$

In the presence of cadmium sulfide on the glass powder with a controlled interfacial area the apparent activation energy of the CdS formation is by a factor of 1.3 lower than that under spontaneous nucleation conditions; E_a is 47.87 kJ/mol in this case.

Equation (4) shows that the partial kinetic order with respect to thiourea is by an order of magnitude lower that that obtained with the use of formal-kinetic Eq. (3) derived for spontaneous nucleation conditions, while the partial orders for trisodium citrate and ammonia are close. Testing this equation showed a good agreement between the experimental and calculated data. Thus, by varying the interfacial area during the CdS deposition from aqueous thiourea solutions in vitro it is possible to completely suppress the process in the reactor volume and to redistribute the sulfide phase onto the surface of the substrate introduced.

As noted above, under conditions of spontaneous nucleation of solid phase, cadmium sulfide is deposited both as a precipitate in the solution volume and as a thin film on a substrate placed in solution. Figure 4 illustrates how the CdS layer thickness varies with the deposition time in the ammonia (1), ammonia-citrate (2), and citrate (3) systems.

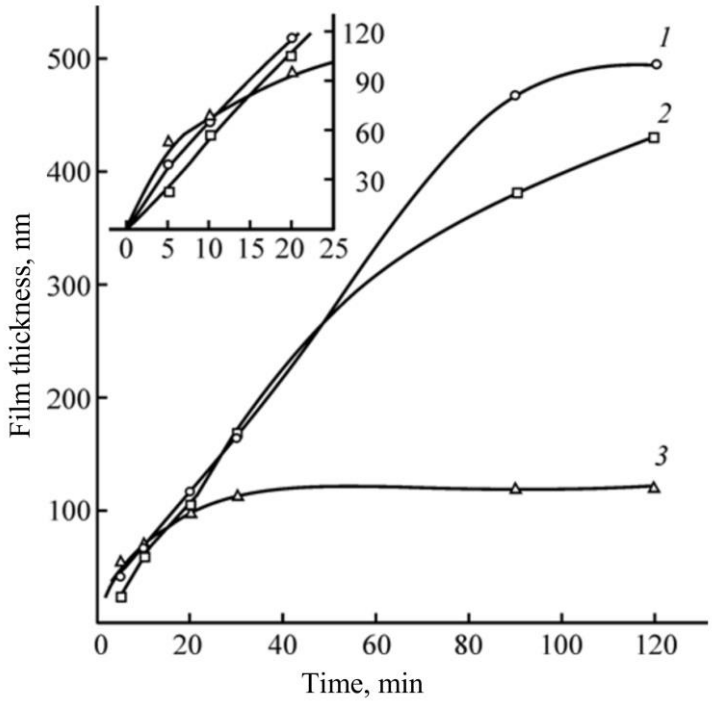

Fig. 4. CdS film thickness as a function of the deposition time in (1) ammonia, (2) ammonia-citrate, and (3) citrate systems. Concentrations of the reactants in the reaction mixture, M: [CdCl2] = 0.02, [Na3Cit] = 0.3, [NH4OH] = 2.0, [CSN2H4] = 0.4; T = 333 K; glass-ceramic substrate. The inset shows the initial period of deposition.

Earlier, we determined the supersaturation level with respect to CdS in the systems examined [18]. The inset in Fig. 4 shows that, in the citrate system, the observed cadmium sulfide film growth in the first minutes somewhat outruns that in the ammonia and ammonia-citrate reaction systems due to a higher supersaturation level ($2.19 \cdot 10^9$ against $3.39 \cdot 10^8$ and $4.47 \cdot 10^8$, respectively [18]).

Figure 5 shows the SEM images of the CdS films formed on the sitall substrate 5 min after the beginning of deposition. The film deposited from the citrate system exhibits a relatively high density and the most uniform size distribution of the cadmium sulfide nanoparticles (Fig. 5a). Specifically in this system the nuclei emerge almost instant at the same time over the entire substrate surface (explosive nucleation) due to significant supersaturation with respect to cadmium sulfide ($2.19 \cdot 10^9$) in the first 5 min. In the initial stage of the synthesis the sitall substrate surface gets covered with an even layer of 20 – 25 nm CdS particles. The film growth in the citrate system is decelerated after the first 20 min of the process, and after 2 h of synthesis its thickness does not exceed 100 nm (Fig. 4). This can be explained by the fact that, in the course of the fast phase formation reaction under high supersaturation conditions, the emergence of CdS nuclei and their growth are redistributed to the solution volume, consequently reducing the probability of the particle adherence to the substrate [20, 21]. The situation is further complicated by kinetic difficulties, in particular, by the attainment of equilibrium by the reaction system (Fig. 1a).

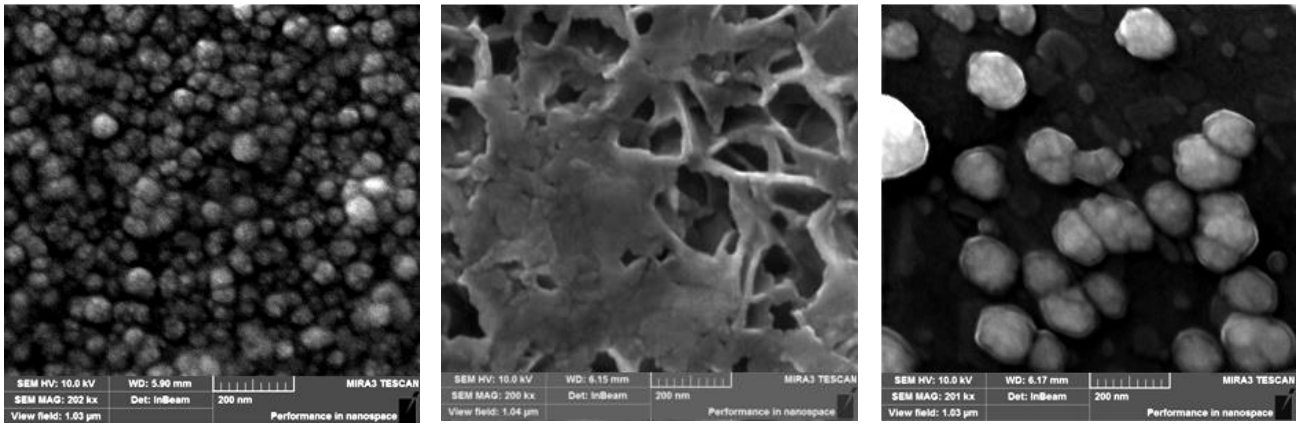

a b c

Fig. 5. SEM images of the CdS layers and their 3D representations 5 min after the onset of the deposition from (a) citrate, (b) ammonia, and (c) ammonia-citrate systems. Concentrations of reactants in the reaction mixture, M: [$CdCl_2$] = 0.02, [Na_3Cit] = 0.3, [NH_4OH] = 2.0, [CSN_2H_4] = 0.4; T = 333 K.

The supersaturation with respect to cadmium sulfide in the ammonia and ammonia-citrate systems was estimated at $3.39 \cdot 10^8$ and $4.47 \cdot 10^8$, respectively. In the ammonia system (Fig. 5b) the cadmium sulfide film fully covers the substrate surface within 5 min, forming a continuous layer of oblong particles measuring ~80 nm on the average. The films deposited from the ammonia bath are the thickest among those deposited from the systems considered (~490 nm after 2 h of synthesis). In the case of the ammonia-citrate system (Fig. 5c) the CdS film is comprised of ~55-nm particles forming aggregates with sizes up to 200 nm during the synthesis. Large particles formed in small amounts at the initial time. The CdS film deposited onto the sitall substrate from the ammonia-citrate bath is slightly thinner (~430 nm) compared to that deposited from the ammonia system, which is consistent with the kinetic curves describing the conversion of the cadmium salt to sulfide (Fig. 1).

In the case of CdS film nucleation under relatively high supersaturation the island phase density and the substrate filling degree is high. When the production of larger crystallites is required, or the energetically most favorable orientation of the film islands, the super-saturation level should be reduced, but the process may take longer time.

Figure 6 shows the 3D images of the most typical fragments of the surface of cadmium sulfide (1×1 μm) deposited within 120 min at 333 K from the reaction mixtures with the use of citrate ions, ammonia, and a mixture of citrate ions with ammonia as complexing agents. The inhomogeneity of the nanocrystalline CdS film surface within the scan was characterized by the arithmetic roughness Ra determining the average deviation of all the points of the roughness profile from the center line. For the cadmium sulfide films deposited from the reaction systems of interest this parameter within the scan increases from 7.9 for the citrate to 45.7 nm for the ammonia-citrate system.

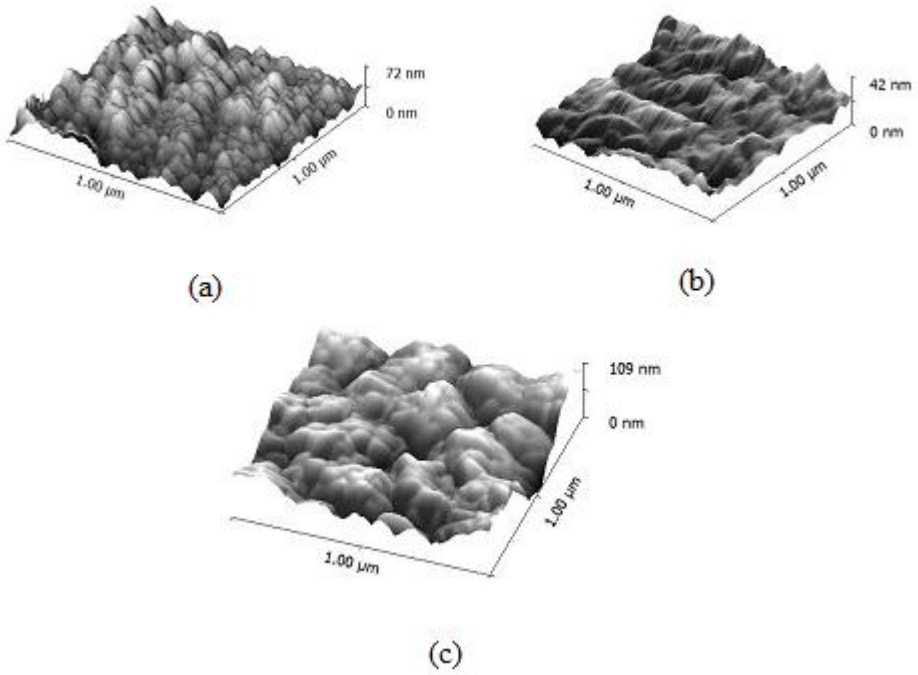

Fig. 6. AFM images of the cadmium sulfide films deposited for 120 min at 333 K from the reaction mixture with the concentrations of the reactants, M: (a) $[CdCl_2]$ = 0.02, $[Na_3Cit]$ = 0.3, $[CSN_2H_4]$ = 0.4, (b) $[CdCl_2]$ = 0.02, $[NH_4OH]$ = 2.0, $[CSN_2H_4]$ = 0.4, and (c) $[CdCl_2]$ = 0.02, $[Na_3Cit]$ = 0.3, $[NH_4OH]$ = 2.0, $[CSN_2H_4]$ = 0.4 (Scan size 1 × 1 μm).

Hydrochemical deposition proceeds in the kinetic region, which makes the temperature a suitable parameter for its effective control [22]. A temperature increase by 20 K under conditions of spontaneous nucleation caused the conversion of the cadmium salt to sulfide to increase from 15 to 70 % (Fig. 2). At the same time, under a controlled solid phase surface area, an increase in the deposition temperature by 15 K onlyleads to exhaustion of the metal salt in the reaction mixture.

The surface area on the glass powder introduced into the reactor can significantly affect not only the metal sulfide deposition rate but also the morphology and properties of the resulting films [21].

4. Conclusion

This study for the first time summarized the kinetic data on the formation of the solid phase of cadmium sulfide under conditions of spontaneous nucleation and interfacial area control as combined with examination of the kinetics of the formation and evolution of CdS films. This allowed establishing a correlation between the supersaturation level created in the reaction mixture and the growth dynamics and morphology of the layers deposited. These results can provide broader opportunities for controlling the layer microstructure, and functional properties.

References

1. Seto S., Nosho Y., Kousho T., Kitani H., Yamada S. *Jpn. J. Appl. Phys.*, 2003, V. 42, N. 10A, 1123.

2. Sorokin S.V., Gronin S.V., Sedova I.V., Rakhlin M.V., Baidakova M.V., Kop'ev P.S., Vainilovich A.G., Lutsenko E.V., Yablonskii G.P., Gamov N.A., Zhdanova E.V., Zverev M.M., Rovimov S.S., Ivanov S.V. *Semiconductors*, 2015, V. 49, N. 3, 331.

3. Li Y., Yuan S.Q., Li X.J. *Mater. Lett.*, 2014, V. 136, 67.

4. Mukherjee A., Satpati B., Bhattacharyya S.R., Ghosh R., Mitra P. *Physica E*, 2015, V. 65, 51.

5. Wang S., Dong W., Fang X., Wu S., Tao R., Deng Z., Shao J., Hu L., Zhu J. *J. Power Sources*, 2015, V. 273, 645.

6. Tomakin M., Altunbas M., Bacaksiz E., Celik S. *Thin Solid Films*, 2012, V. 520, 2532.

7. Antipov V.V., Kukushkin S.A., Osipov A.V. *Phys. Solid State*, 2016, V. 58, N. 3, 629.

8. Belyaev A.P., Rubets V.P., Antipov V.V. *Semiconductors*, 2005, V. 39, N. 2, 189.

9. Samofalova T.V., Semenov V.N., Naumov A.V., Khoviv A.M., Kharin A.N., Lebedeva T.S. *Kondens. Sredy Mezhfaz. Gran.*, 2011, V. 13, N.4, 504.

10. Markov V.F., Maskaev L.N., Ivanov P.N. "Chemical bath deposition of metal sulfides films: modeling and experiment", 218. 1nd edition, *Ekaterinburg*: Ural Branch of Russian Academy of Sciences, 2006.

11. Mokrushin S.G., Tkachev Yu.D. *Kolloidn. Zh.*, 1961, V. 23, N. 4, 438.

12. Uritskaya A.A., Kitaev G.A., Mokrushin S.G. *Kolloidn. Zh.*, 1967, V. 27, N. 5, 767.

13. Chopra K.L., Das S.R. "Thin Film Solar Cells", 288. New York: Springer, 1983.

14. Feitosa A.V., Miranda M.A.R., Sasaki J.M., Araujo-Silva M.A. *Braz. J. Phys.*, 2004, V. 34, N. 2b, 656.

15. Zhang W., Zhang L., Hui, Z. *Solid State Ionics*, 2000, V. 130, 111.

16. Mane R.S., Lokhande C.D. *Thin Solid Films*, 1997, V. 304, 56.

17. Carreón-Moncada I., González L.A., Rodríguez- Galicia J.L., Rendón-Angeles J.C. *Thin Solid Films*, 2016, V. 599, 166.

18. Forostyanaya N.A., Maskaeva L.N., Markov V.F. *Russ. J. Gen. Chem.*, 2015, V. 85, N. 11, 1769.

19. Lurie U.U. "Handbook of Analytical Chemistry", 448. *M.: Chemistry,*1989.

20. Pick H. *Z. Physik*, 1949, V. 126, 12.

21. Kukushkin S.A., Osipov A.V. *Adv. Phys. Sci.*, 1998, V. 168, N. 10, 1083.

22. Bullen C.R., Mulvaney P. *Nano Lett.*, 2004, V. 4, N. 12, 2303.

23. Knorre D.G., Krylova L.F., Muzykantov V.S. "Fizicheskaya khimiya (Physical Chemistry)", 416. *M.*: Vysshaya Shkola, 1990.

24. Schwarzenbach G., Flaschka H. "Complexometric Titrations", 360. 2 ed., *London*: Methuen, 1969.

25. Maskaeva L.N., Kitaev G.A., Zhidkova L.G., Vasyunina L.E. *Zh. Fiz. Khim.*, 1975, V. 69, N. 4, 1042.

Published in the Russian Federation
European Reviews of Chemical Research
Has been issued since 2014.
ISSN: 2312-7708
E-ISSN: 2413-7243
Vol. 10, Is. 4, pp. 122-129, 2016

DOI: 10.13187/ercr.2016.10.122
www.ejournal14.com

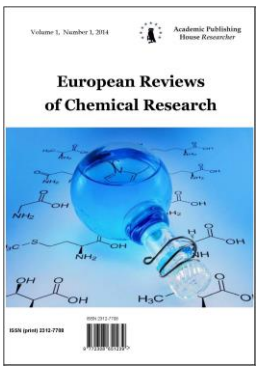

UDC 544.72.05

Kinetic Aspects of Hydrochemical Deposition of Solid Phase Ag_2S

Tatiana V. Vinogradova [a, *], Irina A. Glukhova [a], Larisa N. Maskaeva [a], Vyatcheslav F. Markov [a]

[a] Ural Federal University named after the first President of Russia B.N. Yeltsin, Russian Federation

Abstract

The article considers kinetic aspects study of hydrochemical deposition of solid phase Ag_2S from solutions containing silver nitrate, ammonium hydroxide and sodium citrate at temperatures 303-343 K in the conditions of the spontaneous formation of solid phase.

The authors conclude that:

1. Particular kinetic orders are defined on all components of reaction mixture and activation energy of this process is 37 kJ/mole.

2. In the certain concentration limits formal kinetic equation was derived for the rate of conversion of silver salt into silver sulfide that allows to provide the regulation of the rate of silver sulfide phase formation in the investigated reaction mixture purposefully.

Keywords: hydrochemical deposition, thiocarbamide, kinetic study, silver sulfide, formal kinetic equation, activation energy of chemical reaction.

1. Introduction

Growing interest to silver sulfide Ag_2S is associated with the possibilities of its use in functional electronics due to such properties as low band gap and high chemical stability in the form of nanostructural films, nanocrystals and quantum dots. Thin silver sulfide films are used in galvanic cells and photochemical cells [1, 2], photodetectors [3], solar energy converters [4, 5], sensor technology [6-10].

The practical use of such nanomaterials stimulates the search of possibilities of controlling their production processes. Today there is a great amount of data devoted to the production process of films and silver sulfide residues by both high temperature methods: thermal evaporation [2, 4, 11, 12], electro-deposition [5,13], molecular beam epitaxy (MBE) [14], gamma-irradiation [15], chemical deposition from vapour phase [16], sulfurization [17, 18], and low temperature methods: SILAR method [19, 20], chemical deposition [1, 21-23].

Despite the well-known opinion that it is more practical to use high temperature gas phase methods for the functional materials of optoelectronics, as they give minimum impurities, liquid phase methods have a number of advantages. First of all it is their technological simplicity and possibility of obtaining particles with controlled size.

* Corresponding author
E-mail addresses: t.v.vinog@mail.ru (T.V. Vinogradova), anutan145@mail.ru (I.A. Glukhova), mln@ural.ru (L.N. Maskaeva), v.f.markov@ustu.ru (V.F. Markov)

Among methods of liquid phase Ag_2S production we should emphasize the formation of nanoparticles by chemical deposition from aqueous medium. This is a well-behaved method for the synthesis of both separate sulfides CdS, ZnS, Cu_2Se, In_2S_3, PbSe [24-29], and substitution solid solutions $Cd_xPb_{1-x}S$, $Pb_{1-x}Sn_xSe$, $PbSe_yS_{1-x}$, $Cu_xPb_{1-x}S$, $Cu_2S–In_2S_3$ [30-34] for photodetectors, chemical sensors of toxic gases and heavy metals in aqueous media.

The analysis of publications on chemical deposition of films and powders of silver sulfide by thioamides indicates that there is still a question about mechanism of origin and growth of solid phase particles. To answer these questions it is important to do complex kinetic studies that allow to control and regulate the rate of the conversion of silver salt into sulfide purposefully.

Thus, this work is devoted to the kinetic study of deposition of Ag_2S phase by thiocarbamide in the citrate-ammoniac system and determination of the influence of each component content and temperature on the process rate.

2. Experimental

Kinetic study of chemical deposition of solid phase of silver sulfide Ag_2S by thiocarbamide was carried out in ammonia-citrated system in the conditions of spontaneous formation of solid phase with variations of component concentrations in the reaction mixture in the following ranges, mole/l: $[AgNO_3] = 3\cdot10^{-3}$-$12\cdot10^{-3}$; $[CS(NH_2)_2] = 0.3$-0.5; $[Na_3C_6H_5O_7] = 0.1$-0.3; $[NH_4OH] = 0.5$-4.0. Deposition process was studied in the temperature range 303-343K with the accuracy of temperature control ±0.1 degree. The necessity for temperature standardization and the sequence of reaction component decantation was caused by the fact that the rate of silver sulfide deposition process largely depends on the conditions of nucleation.

To determine the silver content in the solutions Volhard's method was applied with the use of 0.1M ammonium rhodanate solution over ferriammonium sulphates [35]. The titration was made until the appearance of persistent brownish-pink colour of the solution due to the interaction between SCN^- and Fe^{3+} ions. Analitical error was less 0.3%. Taking into account that thiocarbamide connects silver into stable molecular complexes before titration it was broken by sample boiling in concentrated nitric acid.

Excess concentration method suggested by Ostwald was used as a methodology of kinetic study and data interpretation [36, 37]. One of the parameters of the process was changed in each experiment (component concentration, temperature) at constant values of other parameters. Plotting of kinetic curves of deposition of Ag_2S phase was made by evaluation of residual silver in the reaction mixture in certain periods of time, until the equilibrium state in the system.

3. Results and discussion

Kinetic curves of silver salt conversion into sulfide have the typical form for heterogeneous autocatalic processes which occur on the liquid – solid interface boundary (Fig.1). Figure 1 shows that the Ag_2S deposition process has a 5-minute induction period. Due to non-stoichiometric proportion of main components in the reaction system the equilibrium state appears at the time that is different from the time of the beginning of the process.

Particular order on silver salt was determined by graphical method comparing kinetic dependences in different coordinates [36]. It was estimated that in coordinates $\ln [AgNO_3] = f(\tau)$ experimental kinetic curves can be clearly described by the rate equation of the first order that demonstrates the first order of the process on silver salt (Fig. 1).

Kinetic curves of silver nitrate conversion in sulfide in the ammonia-citrated mixture depending on concentration changes of thiocarbamide, ammonium hydroxide, sodium nitrate are given in Fig. 2-4. From experimental data (Fig. 2), it is obvious that reaction between silver salt and thiocarbamide can't be described by whole-number values of stiochiometric coefficients. Particular order determined by the experiment on thiocarbamide $CS(NH_2)_2$ is minus 2.

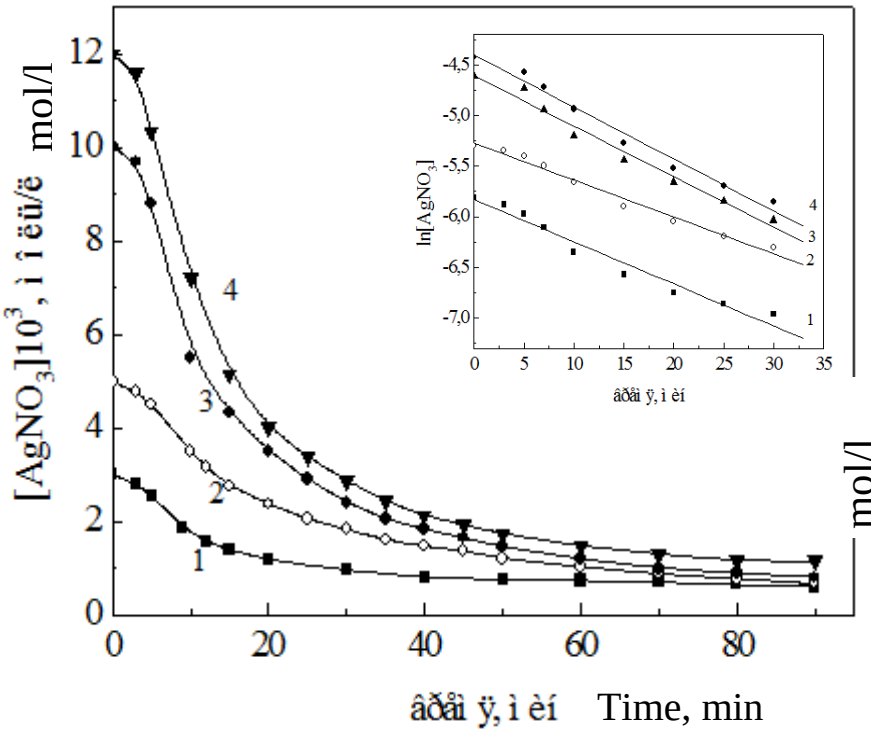

Fig. 1. Kinetic dependences of $AgNO_3$ conversion into sulfide at different initial metal salt concentrations in the reaction mixture, mole/l: 0.003, 0.005, 0.010, 0.012 and evaluation of particilar order of the silver sulfide deposition by thiocarbamide on metal salt. Basic reaction mixture composition, mol/l: $[Na_3C_6H_5O_7]$ = 0.3, $[NH_4OH]$ = 1.0, $[CS(NH_2)_2]$ = 0.4. Process temperature– 323 K.

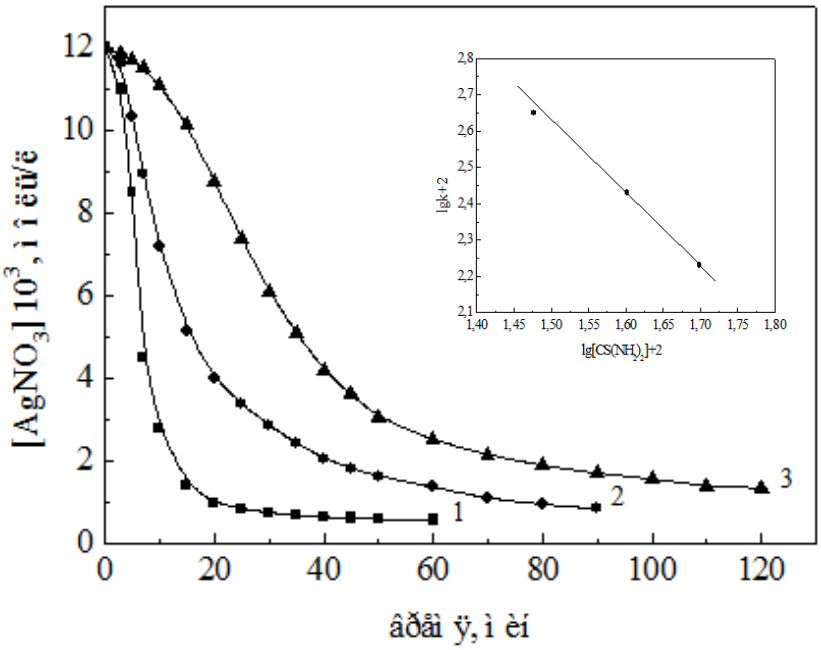

Fig. 2. Kinetic curves of Ag_2S deposition and evaluation of particular kinetic order of silver sulfide deposition on thiocarbamide at its different initial concentrations in reaction mixture, mole/l: 0.3 (1), 0.4 (2), 0.5 (3). Basic solution composition, mole/l: $[AgNO_3]$ = 0.012, $[Na_3C_6H_5O_7]$ = 0.3, $[NH_4OH]$ = 1.0. Process temperature – 323 K.

The values of particular orders on sodium citrate and ammonium hydroxyl show that the concentration changes in the limits mentioned above doesn't influence on deposition process rate.

At the same time increasing of thiocarbamide content in the reaction mixture leads to significant slowing down of the reaction of silver sulfide formation. It is connected with the high value of instability constant of produced complex compound $Ag[CS(NH_2)_2]_3$ ($pk_н$ =13.05) in the system [38].

Fig. 5 shows that with the temperature increasing from 303 K to 343 K the range of the induction period gradually decreases to zero. The dependence of reaction rate constant versus temperature that is described by Arrhenius equation allows to calculate activation energy value and preexponential factor value. Evaluation of these parameters was made by graphic calculation of Arrhenius equation (Fig. 5). As a result activation energy of the Ag_2S formation (E_a) and preexponential factor in Arrhenius equation are 37.0 kJ/mole and $1.15 \cdot 10^4$ $s^{-1} \cdot mole^{-0.7} \cdot l^{0.7}$ correspondingly. The obtained value of activation energy shows that the deposition process predominantly occurs in the kinetic range.

Taking into account the obtained values of particular kinetic orders on reactants and activation energy, formal kinetic equation of conversion rate of silver salt into Ag_2S in the conditions of spontaneous formation of solid phase in citrate-ammoniac system at different reactant contents in the concentration limits mentioned above can be expressed as:

$$W_{Ag_2S} = 1.15 \cdot 10^4 \cdot \exp\left(-\frac{37.0 \cdot 10^3}{8.31 \cdot T}\right) \cdot s \cdot C^{0.3}_{Na_3C_6H_5O_7} \cdot C^{-0.2}_{NH_4OH} \cdot C^{-2.0}_{CS(NH_2)_2} \cdot C_{AgNO_3},$$

where S is the area of the produces solid phase.

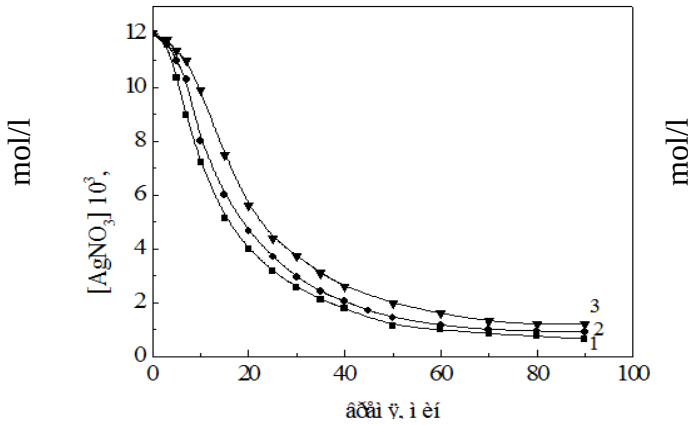

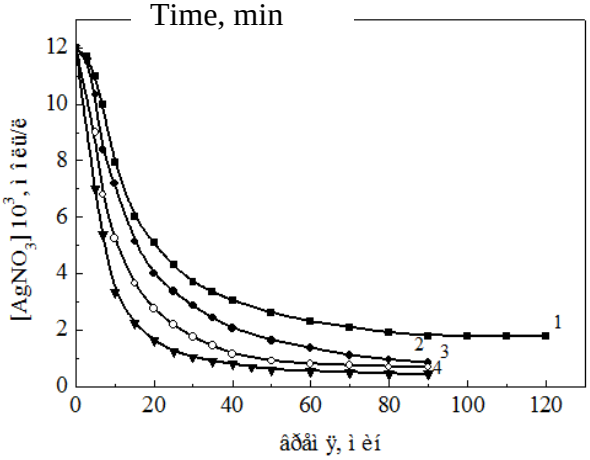

Fig. 3. Kinetic curves of Ag_2S deposition at different initial sodium nitrate concentration $[Na_3C_6H_5O_7]$ in the reaction mixture, mole/l – 0.3 (1), 0.2 (2), 0.1 (3) The solution composition, mole/l: $[AgNO_3]$ = 0.012, $[NH_4OH]$ = 1.0, $[CS(NH_2)_2]$ = 0.4. Process temperature: 323K.

Fig. 4. Kinetic curves of Ag_2S deposition at different initial ammonium hydroxyl $[NH_4OH]$ in the reaction mixture, mole/l – 0.5 (1), 1.0 (2), 2.0 (3), 4.0 (4). The solution composition, mole/l: $[AgNO_3]$ = 0.012, $[Na_3C_6H_5O_7]$ = 0.3, $[CS(NH_2)_2]$ – 0.4. Process temperature – 323 K.

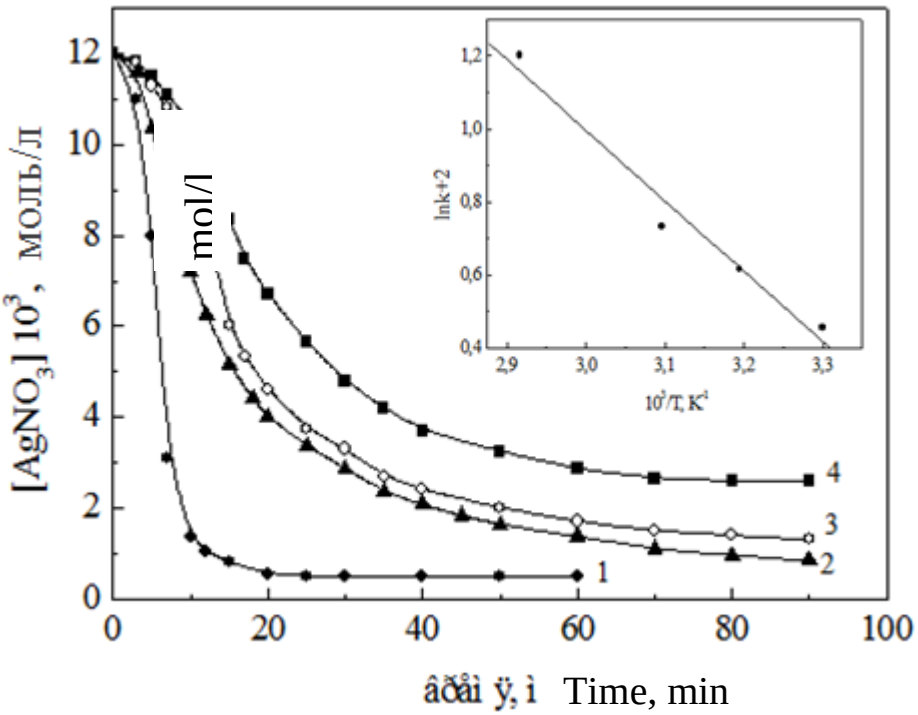

Fig. 5. Kinetic curves of Ag_2S deposition (a) at differsnt process temperature, K: 343 (1), 323 (2), 313 (3), 303 (4) and activation energy evaluation (b). Reaction mixture composition, mole/l: $[AgNO_3]$ = 0.012, $[Na_3C_6H_5O_7]$ = 0.3, $[NH_4OH]$ = 1.0, $[CS(NH_2)_2]$ = 0.4.

Derived formal kinetic equation clearly shows the contribution of each component of the reaction mixture and temperature to the process rate. Thus, on the one hand, increasing of ammonium concentration and particularly thiocarbamide inhibits Ag_2S formation, on the other hand, sodium nitrate influence on the rate is conversed. Probably, it is the result of its intense buffered action, considering that $Na_3C_6H_5O_7$ is a weak tribasic acid salt.

Kinetic equation allows to change the rate of silver sulfide deposition purposefully by varying the component content in the reaction mixture and temperature values. It is an effective instrument for both intensity regulation of nucleation process and particle size of the produced solid phase. Its practical use provides the quick formation of required compound composition of the reaction mixture and allows to decrease the number of searching experiments.

4. Conclusion

1. The complex kinetic study of hydrochemical deposition of silver sulfide in the conditions of spontaneous nucleation of solid phase in the system containing silver nitrate, thiocarbamide, ammonium hydroxide and sodium citrate was made for the first time. The first particular order on silver salt was estimated experimentally. Particukar kinetic orders on thiocarbamide, ammonium hydroxide and sodium nitrate were determined: -2.0, -0.2 and 0.3 correspondingly. Activation energy of the process calculated using Arrhenius equation is 37.0 kJ/mole.

2. Formal kinetic equation of the conversion rate of silver salt into Ag_2S in the conditions of spontaneous nucleation of solid phase was introduced. Its use in a certain concentration limits allows to vary nucleation rate and particle size of the deposited silver sulfide purposefully.

Acknoledgements

The study was financially supported by the Ministry of Education and Science of the Russian Federation in the framework of the governmental task №4.1270.2014/K.

References

1. Meherzi-Maghraoui H., Dachraoui M., Belgacem S., Buhre K.D., Kunst R., Cowache P., Lincot D. Structural, optical and transport properties of Ag_2S films deposited chemically from aqueous solution. *Thin Solid Films*. 1996. Vol.288. Is. 1-2. pp. 217-223.
2. Nasrallah T.B., Dlala H., Amlouk M., Belgacem S., Bernede J.C. Some physical investigations on Ag_2S thin films prepared by sequential thermal evaporation. *Synthetic Materials*. 2005. Vol.151. Is. 3. pp. 225-230.
3. Karashanova D., Nihtianova D., Starbova K., Starbov N. Crystalline structure and phase composition of epitaxially grown Ag_2S thin films. *Solid State Ionics*. 2004. Vol.171. Is. 3-4. pp. 269-275.
4. El-Nahass M.M., Farag A.A.M., Ibrahim E.M., Abd-El-Rahman S. Structural, optical and electrical properties of thermally evaporated Ag_2S thin films. *Vacuum*. 2004. Vol.72. Is. 4. pp. 453-460.
5. Prabhune V.B., Shinde N.S., Fulari V.J. Studies on electrodeposited silver sulphide thin films by double exposure holographic interferometry. *Appl. Surf. Sci.* 2008. Vol.255. Is. 5. pp. 1819-1823.
6. Markov V.F., Vinogradova T.V., Zarubin I.V., Maskaeva L.N. Tonkoplenochnye khimicheskie sensory na osnove $Ag_xPb_{1-x}S_{1-\delta}$ dlya opredeleniya v vozdushnoj srede soderzhaniya NO_2 NO, CO (Thin film chemical sensors based on $Ag_xPb_{1-x}S_{1-\delta}$ for determination of NO_2 NO and CO content in air), *Analytics and Controls*. 2012. Vol.16. No4. pp. 410-414.
7. Umarova N.N., Movchan N.I., Yusupov R.A. and others. Raschet koehffitsienta diffuzii pri ionnom obmene R' (II)/Ag (I) na tonkoplenochnom sorbente PbS (Diffusion coefficient calculation at ionic exchange of Pb (II)/Ag (I) on thin-film sorbent PbS), *Russ, J of Physical Chemistry*. 2000. Vol.74. No9. pp. 1707-1709.
8. Markov V.F., Maskaeva L.N. Poluprovodnikovyj chuvstvitel'nyj ehlement gazoanalizatora oksidov azota na osnove sul'fida svintsa (Swmiconductive sensitive element of nitrogen oxide gas-analyzer based on lead sulfide), *J. of Analytical Chemistry*. 2001. Vol.56. No8. pp. 546-550.
9. Umarova N.N., Movchan N.I., Yusupov R.A., Sopin V.F. Vliyanie kompleksoobrazuyushhikh agentov na ionnyj obmen Ag (I) / R' (II) v tonkikh polikristallicheskikh plenkakh PbS (The influence of complexing agents on ionic exchange of Ag (I) / Pb (II) in thin polycrystalline films of PbS), *Russ. J of Physical Chemistry*. 2002. Vol.76. No8. pp. 1485-1488.
10. Maskaeva L.N., Markov V.F., Vinogradova T.V. and others. Gidrokhimicheskij sintez i svojstva peresyshhennykh tverdykh rastvorov zameshheniya $Ag_xPb_{1-x}S_{1-\delta}$.. (Hydrochemical synthesis and properties of supersaturating solid solutions of substitution of $Ag_xPb_{1-x}S_{1-\delta}$), *The Journal of Surface Investigation. X-ray, Synchrotron and Neutron Techniques*. 2003. No9. pp. 35-42.
11. Karashanova D., Starbova K., Starbov N. Microstructure correlated properties of obliquely vacuum deposited Ag_2S thin films. *J. Optoelectronics & Adv. Mater.* 2003. Vol.5. No.4. pp. 903-906.
12. Korashy E., Abdel-Rahim M.A., Zahed H.E. Optical absorption studies on $AgInSe_2$ and $AgInTe_2$ thin films. *Thin Solid Films*. 1999. Vol.338. Is. 1-2. pp. 207-212.
13. Lekshmi I.C., Berera G., Afsar Y., Miao G.X., Nagahama T., Santos T., Moodera J.. Controlled synthesis and characterization of Ag2S films with varied microstructures and its role as asymmetric barrier layer in trilayer junctions with dissimilar electrodes. *J. Appl. Phys.* 2008. Vol.103. P. 093719.
14. Nozaki H., Onoda M., Yukino K., Kurashima K., Kosuda K., Maki H., Hishita S. Epitaxial growth of Ag_2S films on MgO(001). *J. Sol. State Chem*. 2004. Vol.177. Is. 4-5, pp. 1165-1172.
15. Chen M., Xie Y., Chen H.Y., Qiao Z.P., Qian Y.T. Preparation and Characterization of Metal Sulfides in Ethylenediamine under Ambient Conditions through a γ-Irradiation Route. J. *of Colloid Interf. Sci.* 2001. Vol.237. Is. 1. pp. 47-53.
16. Ali Muhammad, Hamid K., Asif Ali T., Huang Nay M., Wijayantha K.G. Upul, Muhammad M. Synthesis and characterization of silver diethyldithiocarbamate cluster for the deposition of acanthite (Ag_2S) thin films for photoelectrochemical applications. *Thin Solid Films*. 2013. Vol.536. pp. 124-129.
17. Barrera-Calva E., Ortega-López M., Avila-García A., Matsumoto-Kwabara Y. Optical properties of silver sulphide thin films formed on evaporated Ag by a simple sulphurization method. *Thin Solid Films*. 2010. Vol.518. pp. 1835-1838.

18. Agbo P.E., Nwofe P.A. Structural and Optical Properties of Sulphurised Ag_2S Thin Films. *Int. J. Thin. Fil.* 2015. Vol.4. No.1. pp. 9-12.

19. Pathan H.M., Salunkhe P.V., Sankapal B.R., Lokhande C.D. Photoelectrochemical investigation of Ag_2S thin films deposited by SILAR method. *Materials Chemistry & Physics*. 2001. Vol.72. Is. 1. pp. 105-108.

20. Auttasit T., Kun-Lun W., Hao-Yu T., Ming-Way L., Gou Jen W. Ag_2S quantum dot-sensitized solar cells. *Electrochem. Commun.* 2010. Vol.12. Is. 9. pp. 1158-1160.

21. Dhume S.S., Lokhande C.D. Preparation and characterization of chemically deposited Ag_2S films. *Solar Energy Materials & Solar Cells*. 1992. Vol.28. Is. 1. pp. 159-166.

22. Núñez Rodríguez A., Nair M.T.S., Nair P.K. Structural, optical and electrical properties of chemically deposited silver sulfide thin films. *Semicond. Sci. Technol.* 2005. Vol.20. No.6. pp. 576-585.

23. Jadhav U.M., Gosavi S.R., Patel S.N., Patil R.S. Studies on Characterization of Nanocrystalline Silver Sulphide Thin Films Deposited by Chemical Bath Deposition (CBD) and Successive Ionic Layer. *Arch. Phys. Res*. 2011. Vol.2. No.2. pp. 27-35.

24. Forostyanaya N.A., Maskaeva L.N., Markov V.F. Vliyanie prirody liganda na granichnye usloviya obrazovaniya i morfologiyu nanokristallicheskikh plenok CdS (The influence of ligand nature on the boundary conditions of formation and morphology of nanocristalline films of CdS), *J. of General Chemistry*. 2015. Vol.85. No10. pp. 1596-1601.

25. Maskaeva L.N., Shemyakina A.I., Markova V.F., Saryeva R.Kh. Prognozirovanie uslovij himicheskogo osazhdeniya i mikrostruktura nanokristallicheskih plenok sul'fida cinka (Prognostication of chemical deposition conditions and microstructure of nanocristalline zinc sulphide films), *J. Applied Chem*. 2015. Vol.88. No9. pp. 115-125.

26. Fedorova E.A., Maskaeva L.N., Markov V.F., Ermakov A.N., Samigulina R.F. Gidrokhimicheskij sintez i termicheskaya ustojchivost' nanokristallicheskikh plenok i osadkov selenida medi(I) (Hydrochemical synthesis and thermal stability of nanocrystalline films and residues of copper (I) selenide), *J. of Inorganic Chemistry*. 2015. Vol.60. No11. pp. 1432-1438.

27. Tulenin S.S., Markov V.F., Maskaeva L.N. Vliyanie termicheskogo otzhiga na strukturu i sostav nanostrukturirovannogo sul'fida indiya (III) (The influence of thermal annealing on structure and composition of nanostructured indium (III) sulfide), *Non-ferrous Metals*. 2015. No4. pp. 28-32

28. Smirnova Z.I., Bakanov V.M., Maskaeva L.N., Markov V.F., Voronin V.I.. Vliyanie jodsoderzhashhej dobavki na sostav, strukturu i morfologiyu khimicheski osazhdennykh plenok selenida svintsa (The influence of iodine addition on composition, structure and morphology of chemically deposited films of lead selenides), *Physics of the Solid States*. 2014. Vol.56. Is. 12. pp. 2468-2474.

29. Markov V.F., Alekseeva T.A., Maskaeva L.N. Osobennosti gidrokhimicheskogo osazhdeniya plenok sul'fidov i selenidov metallov (Features of hydrochemical deposition of metal sulfides and selenides films), *Butlerovskie Soobshch*. 2015. Vol.41. No1. pp. 8-21.

30. Markov V.F., Maskaeva L.N., Porkhachev M.Yu., Mokrousova O.A. Termicheskaya i radiatsionnaya ustojchivost' IK-detektorov na osnove plenok tverdykh rastvorov $Cd_xPb_{1-x}S$ (Themal and radioactive stability of IR-detectors based on solid solution films of $Cd_xPb_{1-x}S$), *Fire and Explosion Safety*. 2015. Vol.24. No9. pp. 67-73.

31. Mukhamedzyanov H.N., Maskaeva L.N., Markov V.F. Sravnitel'nye fotoehlektricheskie kharakteristiki nanostrukturirovannykh plenok $Pb_{1-x}Sn_xSe$, poluchennykh sovmestnym i poslojnym osazhdeniem PbSe i SnSe (Comparative photovoltaic characteristics of nanostructured $Pb_{1-x}Sn_xSe$ films obtained by co-deposition and by layer-by-layer deposition of PbSe and SnSe), *Semiconductiors*. 2014. Vol.48. No2. pp. 278-282

32. Sergeeva A.S., Markov V.F., Maskaeva L.N. Termosensibilizatsiya khimicheski osazhdennykh plenok na osnove tverdykh rastvorov $PbSe_yS_{1-x}$ (Thermal sensitation of chemically deposited films based on solid solutions of $PbSe_yS_{1-x}$), *Glass Physics and Chemistry*. 2014. Vol.40. No2. pp. 298-307.

33. Maskaeva L.N., Markov V.F., Voronin V.I., Gusev A.I. Hydrochemical synthesis, structure and properties of films of supersaturated substitutional $Cu_xPb_{1-x}S$ solid solutions. *Thin Solid Films*. 2004. Vol.461. pp. 325-335.

34. Tulenin S.S., Markov V.F., Maskaeva L.N., Kuznetsov M.V. Gidrokhimicheskoe osazhdenie i issledovanie tonkikh plenok v sisteme $Cu_2S–In_2S_3$ (Hydrochemical deposition and study of thin films in the system $Cu_2S–In_2S_3$), *Butlerovskie Soobshch*. 2013. Vol.33. No1. pp. 97-103.

35. Sharlo G. Metody analiticheskoj khimii. Kolichestvennyj analiz neorganicheskikh soedinenij (Methods of analytical chemistry. Quantitative analysis of inorganic compounds). Moscow., Leningrad.: Khimiya. 1965. 976 p.

36. Mejtis L. Vvedenie v kurs khimicheskogo ravnovesiya i kinetiki (Introduction to the course of chemical equilibrium and kinetics). Moscow: Mir. 1984. 484 p.

37. Knorre D.G., Krylov L.F., Muzykantov V.S. Fizicheskaya khimiya (Physical chemistry), Moscow: Vysshaya Shkola. 1990. 416 p.

38. Pyatnitskij I.V., Sukhan V.V. Analiticheskaya khimiya serebra (Analytical chemistry of silver), Moscow: Nauka. 1975. 264 p.